ACS OMEGA

Open Access



http://pubs.acs.org/journal/acsodf

Article

# Exploring New Schiff Bases: Synthesis, Characterization, and Multifaceted Analysis for Biomedical Applications

*Published as part of ACS Omega virtual special issue "3D Structures in Medicinal Chemistry and Chemical Biology".*

Priteshkumar M. Thakor, Jatin D. Patel,* Rajesh J. Patel, Sunil H. Chaki, Ankurkumar J. Khimani, Yati H. Vaidya, Anita P. Chauhan, Amit B. Dholakia, Vishant C. Patel, Ankitkumar J. Patel, Nirav H. Bhavsar, and Hiteshkumar V. Patel

Cite This: *ACS Omega* 2024, 9, 35431−35448

Read Online

ACCESS | Metrics & More | Article Recommendations

**ABSTRACT:** The current work aims to generate novel Schiff bases by reacting substituted aldehydes with amine derivatives catalyzed by a natural acid. The developed compounds underwent diverse physicochemical analyses including liquid chromatography−mass spectrometry, Fourier transform infrared spectroscopy, scanning electron microscopy, $^{1}$H- and $^{13}$C-nuclear magnetic resonance, and X-ray diffraction. Furthermore, differential thermogravimetric, thermogravimetric, and differential thermal analysis techniques were employed in a nitrogen-free environment to determine kinetic parameters. These data were then used in model-free isoconversional methods (e.g., Friedman, Kissinger−Akahira−Sunose, and Flynn−Wall−Ozawa). The Schiff bases were evaluated for their *in vitro* and *in silico* $\alpha$-amylase inhibitory activity. Schiff base-2 displayed the highest inhibition compared with the reference drug acarbose. In comprehensive MTT assay cytotoxicity investigations, both Schiff bases showed strong anticancer capabilities against the human lung cancer cell line (A549). Moreover, this study demonstrated effectiveness of synthetic compounds in screening *Caenorhabditis elegans* for anti-Alzheimer's and stress resistance properties. The simplicity of its biology allowed precise evaluation of the effect of compounds on neuronal function and stress response. This research enhances drug discovery efforts for Alzheimer's and stress-related disorders, potentially improving patient outcomes.

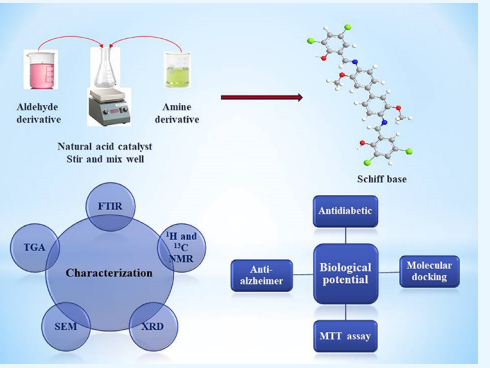


## 1. INTRODUCTION

Schiff bases play a crucial role in synthesizing various industrially and physiologically beneficial chemicals through closure, cycloaddition, and replacement reactions.[1,2] Additionally, they exhibit a broad spectrum of well-known biological effects,[3−5] including anti-inflammatory, allergen inhibition, radical scavenging, pain-relief, and antioxidant abilities.[6−8]

The swift progressions in pharmaceutical and medicinal chemistry have diverted the attention of scientists toward the development of drugs, even for intricate conditions such as diabetes mellitus, a critical global health concern that emerges from aberrant insulin production.[9−11] Schiff bases have demonstrated encouraging results across a range of research domains, as they investigate their insulin-mimetic characteristics. Schiff bases have notably exhibited antidiabetic potential, as demonstrated by Szklarzewick's group.[12]

Cancer poses significant challenges globally due to its tendency to develop drug resistance and inadequate response to cytotoxic treatments.[13,14] Researchers are actively seeking novel drugs with reduced systemic toxicity and improved cytotoxicity. Numerous scholarly articles have emphasized the anticancer properties of Schiff bases, utilizing diverse human tumor cell lines.[15,16]

The utilization of *Caenorhabditis elegans* (*C. elegans*) as a model organism holds immense promise in screening synthetic compounds for their potential anti-Alzheimer's and stress resistance properties.[17] With its well-defined biology and simple nervous system, *C. elegans* offers a unique platform for precise assessment of compound efficacy and toxicity. Through systematic experimentation, researchers can expose the worms to a diverse array of synthesized compounds, evaluating their

Received: February 29, 2024
Revised: April 18, 2024
Accepted: May 8, 2024
Published: June 24, 2024

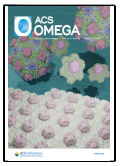

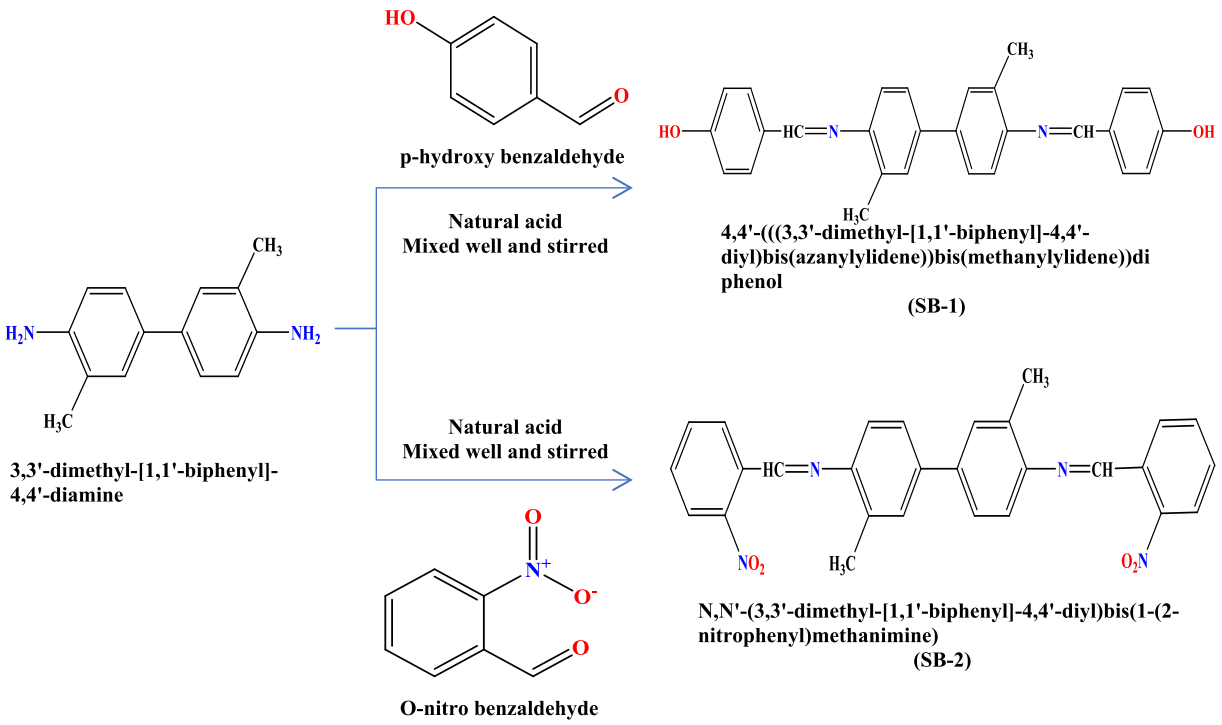


**Figure 1.** Synthesis of Schiff base-1 (SB-1) and Schiff base-2 (SB-2).

effects on stress response and neuronal function. This approach not only provides valuable insights into the mechanisms of action of these compounds but also aids in the identification of novel therapeutic interventions for Alzheimer's disease and stress-related disorders.[18]

In the present scenario, researchers are increasingly focusing on reducing chemical waste, reaction time, and the use of toxic compounds in organic transformations by adopting green catalysts. Green synthesis involves substituting harmful and costly catalysts with readily available biocatalysts.[19,20] In this context, the aim of this work is to utilize environmentally friendly methods and reagents to enhance the production of Schiff bases despite numerous existing techniques. Specifically, we here employed a green approach to individually couple the amine derivative 3,3′-dimethyl-[1,1′-biphenyl]-4,4′-diamine with *o*-nitro benzaldehyde and *p*-hydroxy benzaldehyde, yielding two distinct Schiff bases, Schiff base-1 (SB-1) and Schiff base-2 (SB-2). This eco-friendly reaction offers advantages over traditional reflux methods, including higher product yields, moderate reaction conditions, and simplified work processes.[21,22] The Schiff bases that were synthesized were then thoroughly characterized using a range of physicochemical techniques, including melting point determination, thin layer chromatography (TLC), Fourier transform infrared spectroscopy (FTIR), nuclear magnetic resonance (NMR) spectroscopy ($^1$H and $^{13}$C), scanning electron microscopy (SEM), liquid chromatography−mass spectrometry (LC-MS/MS), and X-ray diffraction (XRD).[23−26] Thermal characterization was conducted by collecting thermogravimetric (TG), differential thermal analysis (DTA), and differential thermogravimetric (DTG) thermocurves under a nitrogen atmosphere, with kinetic parameters computed based on the thermocurve data.[27] Furthermore, the synthesized Schiff bases' potential biological activities were explored including *in vitro* antidiabetic property, molecular docking study, and *in vitro* cytotoxicity assays.[28,29] A549 human lung cancer cells were utilized to assess the cytotoxicity of the compounds, revealing promising results in terms of the cytotoxic effects against lung cancer cells. Additionally, current study utilized *C. elegans* as a model organism to assess the synthetic compounds' potential anti-Alzheimer's and stress resistance properties. Through systematic experimentation, we evaluated their effects on the worm's stress response and neuronal function, highlighting the significance of *C. elegans* in drug discovery and toxicity research.[30] This research contributes to identifying novel therapeutic interventions for Alzheimer's disease and stress-related disorders, offering potential improvements in patient outcomes.

## 2. MATERIALS AND METHODS

**2.1. Materials.** The materials used to develop Schiff bases include 3,3′-dimethyl-[1,1′-biphenyl]-4,4′-diamine (minimum assay, 97.5%, Spectrochem), *o*-nitro benzaldehyde, and *p*-hydroxy benzaldehyde (minimum assay, 98%, Sigma-Aldrich), and all the solvents used were purchased from Merck, Loba, SRL, and Spectrochem and also tightly packed in airtight bottles to reduce evaporation from the atmosphere. In addition, they were distilled before use. Upon arrival, all compounds were used without further purification, as they were of analytical quality. The lemons used to make the juice came from a local store.

**2.2. Instrumental Methods.** The melting points of the synthesized Schiff bases were determined using Analab's melting point equipment. The unit crystal structure of the product was determined by X-ray diffraction (XRD) utilizing Cu−K$\alpha$ radiation and a Rigaku Ultima IV Powder X-ray diffractometer. A PerkinElmer FTIR L160000T spectrometer was used to record the FTIR spectrum as part of the physicochemical characterization process. JEOL ECZ600R 600 MHz $^1$H NMR and $^{13}$C NMR spectra were acquired with THF or DMSO-$d_6$ as solvents. Scanning electron microscopy was performed using the Quanta FEG 250 model, a field emission


https://doi.org/10.1021/acsomega.4c02007
ACS Omega 2024, 9, 35431−35448

scanning electron microscope. Mass spectrometry data were acquired using a Shimadzu LC-MS/MS 8050. Thermal analysis, including TG, DTA, and DTG curves, was conducted by using the Seiko SII-EXSTAR TG/DTA-7200 thermal analyzer. The thermocurves were measured in an inert nitrogen atmosphere keeping a flow rate of 100 mL·min$^{-1}$. The measurements were done for three different heating rates, 10, 15, and 20 K·min$^{-1}$. In all the measurements, the starting sample weight was taken between 10 and 12 mg. The thermocurves were recorded in the temperature range of ambient and 430 K.

**2.3. Protocol for the Synthesis of Schiff Base-1 (SB-1) and Schiff Base-2 (SB-2).**[31,32] Ten millimoles of 4-hydroxy benzaldehyde and 2-nitro benzaldehyde was dissolved separately in a small amount of absolute ethanol in two different beakers. These solutions were gradually poured into two separate beakers containing a solution of 5 mmol of 3,3′-dimethyl-[1,1′-biphenyl]-4,4′-diamine dissolved in ethanol, with constant stirring. Then, while the mixtures were stirred at room temperature, 2 mL of freshly squeezed lemon juice was added to each reaction. After that, the reaction mixture was constantly mixed while TLC was used to track and record the reaction's progress. The outcome yielded a solid tea-green product for Schiff base-1 (SB-1) and a yellow-colored product for Schiff base-2 (SB-2). These products were then filtered, washed with water, and subjected to recrystallization using DMSO. The synthetic pathway of Schiff base-1 and Schiff base-2 is illustrated in Figure 1.

**2.4. Biological Studies.** *2.4.1. Antidiabetic Activity. 2.4.1.1. In Vitro α-Amylase Inhibitory Activity.* The α-amylase inhibition *in vitro* experiment was conducted according to the techniques described in refs 33−35. The amylase enzyme solution in this configuration was made in 0.1 M phosphate buffer with a pH of 6.9. A 0.5 mL portion of a Schiff base solution at a concentration of 1 mg/mL was added to start the enzyme reaction. A 1% starch solution (0.5 mL) in 0.1 M phosphate buffer at pH 6.8 was added after a 10 min incubation period at 25 °C. An extra 10 min was spent keeping the reaction mixture at 25 °C. A parallel procedure was conducted for the control, where 0.5 mL of buffer was substituted for the enzyme solution. Dinitrosalicylic acid reagent was added to both the control and test reactions after they had been incubated for 10 min. This was followed by a further 10 min of incubation in a boiling water bath. After the reaction mixture cooled, the absorbance at 540 nm was measured with a UV−visible spectrophotometer. A specific mathematical calculation was utilized to calculate the inhibition percentage of the α-amylase enzyme.

$$\%\text{inhibition} = \frac{\text{absorbanceofcontrol} - \text{absorbanceofsample}}{\text{absorbanceofcontrol}} \times 100 \quad (1)$$

The kinetic parameter $V_{max}$ and $K_m$ values of both α-amylase inhibitors were calculated by the Lineweaver−Burk equation and graph fitting analysis using Microsoft Excel version 2019.[36−38]

*2.4.1.2. Molecular Docking Study.* Molecular docking was performed on the protein−ligand complexes using Auto Dock Vina.[39] To get the 3D model of the RCSB Protein Data Bank's Wild-Type Human Pancreatic Alpha-Amylase (PDB ID: 4X9Y), we utilized AutoDockTools 1.5.6. Various components, including water and solvent molecules, the bonded ligand, polar hydrogen, and partial charges, had to be removed. Storage of the generated structure was accomplished by using the Auto Dock PDBQT format. ChemBio3D Ultra 14.0 software was utilized to optimize the structures of the synthesized Schiff bases (SBs) and the reference medication, acarbose, using the Merck Molecular Force Field (MMFF94) technique.[40] Following optimization, the Schiff bases' mol2 format was converted to PDBQT files using AutoDockTools 1.5.6.[41]

Docking of the Schiff base model was conducted to elucidate their binding mechanisms with the active sites of macromolecular targets. For this operation, the Lamarckian genetic algorithm was run with its default settings. The receptor's autogrid settings were set to 40 in all dimensions, with a grid spacing of 0.375 Å and grid centers of −8.289 in *X*, −5.639 in *Y*, and 15.835 in *Z*.[42] The outcomes were evaluated based on free binding energy, and the distances between specific atoms or molecules and amino acids were examined using the Biovia Discovery Studio Visualizer.

*2.4.2. In Vitro Cytotoxicity Studies. 2.4.2.1. In Vitro Cytotoxicity Study by Using Human Lung Cancer Cell Line A549. 2.4.2.2. Cell Culture and Cell Line.* The A549 human lung cancer cell line was obtained from the National Centre for Cell Science (NCCS) in Pune, India. DMEM/F12, fetal bovine serum, penicillin (50 μg/mL), and streptomycin (50 μg/mL) were provided by Gibco, Invitrogen, located in CA, USA. The cells were cultivated at 37 °C in a humidified atmosphere with 5% carbon dioxide in DMEM/F12 media supplemented with 10% fetal bovine serum, 50 μg/mL penicillin, and 50 μg/mL streptomycin. Until the cells attained confluence, the medium was changed every 3 days, at which time they were subcultured.[43]

*2.4.2.3. Antiproliferative Test.* The antiproliferative assay, adapted from Gajera et al.,[44] involves evaluating the compatibility of the SB compounds with some adjustments. Following the addition of the Schiff base, the culture medium was diluted with water to achieve the required concentrations. Preparation of new batches of compound solutions was carried out immediately before their use. A 24 h incubation period was followed by the placement of exponentially growing cells (10,000 cells per well) onto 96-well plates with complete media. Following this, the cells were cultured for a further 24 h while being exposed to varying quantities of the test samples. Subsequently, each treated well received 5 μL of MTT (5 mg/mL), and the cells were grown for 3−4 h at 37 °C in a $CO_2$ incubator to produce formazan crystals, resulting in a purple color. The incubated media from every well were carefully collected and mixed with 100 μL of DMSO, which is suitable for tissue culture. Using a microplate reader, we measured the absorbance of the final suspension at 570 nm. Cell viability is then determined using the optical density (OD) data of the antiproliferative assay and an equation that is provided.

$$\%\text{cell viability} = \frac{\text{absorbance value for sample nanoparticle-treated cells}}{\text{absorbance value of control cells}} \times 100 \quad (2)$$

$$\%\text{cell inhibition} = (100 - \%\text{cell viability}) \quad (3)$$

*2.4.2.4. In Vitro Cytotoxicity Studies by Using C. elegans. 2.4.2.5. C. elegans Strains and Their Maintenance.* The strains of *C. elegans* used in this research included N2 Bristol



https://doi.org/10.1021/acsomega.4c02007
ACS Omega 2024, 9, 35431−35448

Table 1. Physicochemical Characterization Data of the Schiff Bases

| compound | molecular formula | molecular weight (g/mol) | color | melting point (°C) | yield |
|---|---|---|---|---|---|
| Schiff base-1 | $C_{28}H_{24}N_2O_2$ | 420.51 | tea green | 260−270 | 85.22% |
| Schiff base-2 | $C_{28}H_{22}N_4O_4$ | 478.51 | yellow | 200−220 | 95.15% |

(wild-type) and CL4176 (Alzheimer's disease model). These worms were cultured and kept at 16 °C in nematode growth medium (NGM). NGM-agar media were prepared by blending agar, NaCl, peptone, $CaCl_2$, $MgSO_4$, $KPO_4$ buffer, and cholesterol. NGM plates were then made and seeded with *Escherichia coli* strain OP50, which acts as a food source for *C. elegans*. *E. coli* OP50, a uracil auxotroph, was grown overnight in Luria−Bertani (LB) at 37 °C in a shaking incubator. The cultured *E. coli* OP50 was placed as a spot in the middle of each plate and allowed to air-dry. The worms were subsequently transferred from the master plate to the NGM plates. All *C. elegans* strains and *E. coli* OP50 were obtained from the *Caenorhabditis* Genetics Centre (CGC) at the University of Minnesota in the United States.

*2.4.2.6. Worm Synchronization.* The synchronization process is critical for *C. elegans* experiments to ensure that the analysis is precise and free of errors. The maintained *C. elegans* is always in various states of the cell cycle. Any experiment requires that all of the worms be at the same stage of their life cycle, which is accomplished through synchronization. It can be done in a variety of ways, the most frequent of which is bleaching. Bleaching can cause the outer cuticle of the worm's body to break apart, allowing gravid worms to release their eggs. The eggshells that cover the eggs prevent them from bleaching. Synchronization requires a huge population of worms.[45]

Once a large number of eggs or gravid adults were visible, the worms were moved to new NGM plates and allowed to continue growing. This was followed by rinsing them with M9 buffer, which consisted of 5 g of NaCl, 3 g of $KH_2PO_4$, 6 g of $Na_2HPO_4$, and 1 mL of 1 M $MgSO_4$ diluted to 1 L with distilled water. After spinning the sample at 1200 rpm for 2 min, the liquid on top was removed and replaced with M9 buffer. To eradicate bacterial contamination, the washing operation was done 4 to 5 times. The alkaline hypochlorite solution was created for the bleaching process by combining 1 N NaOH and 5% NaOCl. The bleaching solution was applied to the washed worms and vortexed for 5 to 7 min. After the eggs were collected, the M9 buffer was injected again to neutralize the bleach effect. The eggs were rinsed again with M9 buffer until the bleach smell was gone. After washing with M9 buffer, the eggs were resuspended in an S-basal solution and incubated overnight on a rocker at 20 °C. The eggs hatched the next day in the L1 stage. The L1 worms were subsequently moved to a fresh NGM plate with *E. coli* OP50 and allowed to incubate until they reached the L4 developmental stage.

*2.4.2.7. LD50 to Determine Lethal Doses.* After autoclaving and before pouring, the compound was added to NGM to make the experimental plates. Worms were subjected to synthetic substances at doses varying from 10 to 100 $\mu$g/mL to determine the $LD_{50}$. The number of deceased worms was recorded until all of the worms had perished. The concentration at which 50% of the worms died was considered as $LD_{50}$ of respective compounds. The effect of various synthetic compounds was explored in *C. elegans* by the addition of compounds along with NGM agar at a dose according to 1/10th of $LD_{50}$ values.[46]

*2.4.2.8. Stress Resistance Assays.* The stress resistance capability sheds light on the interaction of internal and external pressures as well as biological processes at the cellular and subcellular levels. Stresses such UV radiation, cold stress, oxidative stress, heat stress, a lack of oxygen, and high oxygen levels all cause the activation of stress factors in *C. elegans*. In this study, the investigation focused on the stress response concerning thermal (heat) and oxidative stress. Synchronized L4 wild-type worms were utilized for the stress resistance assay. Initially, the worms were permitted to reach adulthood in both experimental NGM plates and control plates. Subsequently, after the treatments, the worms underwent thermal and oxidative stress tests.

For the thermal stress assay, the temperatures of the treated and control worms were kept at 20 °C. Thermal stress was induced by exposing all worms to 35 °C for a duration of 12 h. The number of deceased worms was tallied every 2 h throughout the 12 h period. Subsequently, a survival curve was generated to compare the stress resistance between the treated and control worms.

For the oxidative stress assay, the treated and control worms underwent a rinsing step with M9 buffer before being subjected to oxidative stress resistance testing. After being removed from the plates, the worms were centrifuged at 1200 rpm for 2 min at 4 °C, repeated three to four times. Subsequently, the worms were immersed in a 20 mM hydrogen peroxide ($H_2O_2$) solution for a maximum of 2 h. Worms were given 16 h to recuperate after being exposed to hydrogen peroxide before being placed on new NGM plates and placed in an incubator set at 20 °C. We calculated the proportion of worms that survived oxidative stress by counting the number of worms that survived after recovery.

*2.4.2.9. Paralysis Assay.* The paralysis assay was used to determine whether compounds may be used to treat Alzheimer's disease. The transgenic CL4176 *C. elegans* contains a human A1−42 transgene that is heat-inducible and expressed in muscle cells. The age-synchronized CL4176 worms were first reared under compound treatment at 16 °C before being used in the paralysis assay. Along with the treated worms, the control worms were also subjected to a 20 h temperature shift to 25 °C. The paralysis was caused by raising the temperature of the worms to a nonpermissive level, which activated the amyloid-$\beta$ (A) in their muscle cells. The worms were examined every 2 h until they were all paralyzed after an incubation period of 1 day at 25 °C. Worms were considered paralyzed if they were alive but unresponsive to any mechanical stimuli.

## 3. RESULTS AND DISCUSSION

**3.1. Chemistry.** The current Schiff bases are produced via the condensation reaction of 3,3′-dimethyl-[1,1′-biphenyl]-4,4′-diamine with two distinct aldehydes, 4-hydroxy benzaldehyde and 2-nitro benzaldehyde, in a 1:2 molar ratio utilizing natural acid-catalyzed synthesis. The physical and molecular characteristics of each synthesized compound are listed in


https://doi.org/10.1021/acsomega.4c02007
ACS Omega 2024, 9, 35431−35448

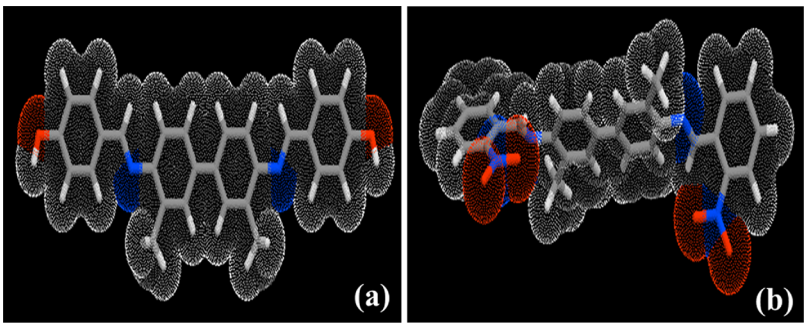


**Figure 2.** (a, b) 3D structures of SB-1 and SB-2, respectively. Dot and stick model: red tubes, oxygen; gray tubes, carbon; blue tubes, nitrogen; white tubes, hydrogen.

Table 1. Figure 2a,b represents 3D structures for Schiff base-1 and Schiff base-2, respectively.

**3.2. Characterization.** *3.2.1. FTIR.* The compounds that were produced had their infrared spectra examined in the 450−4000 $cm^{-1}$ range (Figure 3a,b). The presence of $\nu$(C═N) azomethine stretching vibrations was confirmed by the detection of medium absorption peaks at 1606 $cm^{-1}$ for SB-1 and 1623 $cm^{-1}$ for SB-2, which indicate the establishment of Schiff base linkage. Furthermore, the lack of aldehyde- and amine-specific C═O and $NH_2$ stretching vibrations, respectively, indicates the production of the imine bond, which is important to the Schiff base reaction. In SB-1, a strong peak at 1320 $cm^{-1}$ was associated with $\nu$(C−OH), while in SB-2, a prominent peak at 1530 $cm^{-1}$ was linked to $\nu$(C−NO). Moreover, medium-intensity peaks at 1120 $cm^{-1}$ for SB-1 and 1122 $cm^{-1}$ for SB-2 were attributed to the (Ph-N) group. Broad signals observed around 3000 $cm^{-1}$ in both the compound's IR spectra were attributed to aromatic protons.

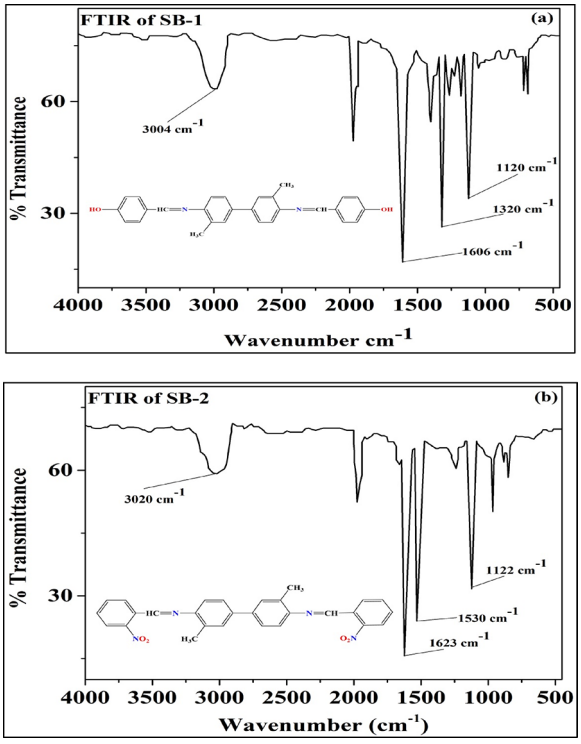


**Figure 3.** (a, b) FTIR spectra of Schiff base-1 and Schiff base-2, respectively.

*3.2.2. $^1H$ NMR.* Using DMSO-$d_6$ as the solvent, the $^1H$ NMR spectra of the derived compounds (Figure 4a,b) were recorded. In the case of SB-1, a signal was detected at 8.68 ppm, and for SB-2, it appeared at 8.80 ppm, indicating the presence of $\alpha$ hydrogen in the imine linkage (HC═N). The signals detected for SB-1 and SB-2, respectively, at 2.53 and 2.13 ppm were determined to be $CH_3$ resonances. These compounds showed aromatic rings, as evident from multiple signals between 6.57 and 7.86 ppm for SB-1 and 6.51 and 8.11 ppm for SB-2, corresponding to aromatic proton resonance. Furthermore, a signal at 10.15 ppm in SB-1 indicated the presence of −OH functionality.

*3.2.3. $^{13}C$ NMR.* Figure 5a,b shows the $^{13}C$ NMR spectra of the produced compounds in DMSO-$d_6$. In the spectrum of SB-1, the signal at 162.79 ppm indicated the carbon linked to the hydroxyl group, while in the spectrum of SB-2, the signal at 165.79 ppm indicated the carbon linked to the nitro group. The $-CH_3$ group carbon contributed to the signal observed at 17.95 ppm in SB-1 and at 18.43 ppm in SB-2. The signals in the spectra of SB-1 ranging from 110.60 to 130.14 ppm were indicative of aromatic carbons in the benzene ring and 111.98 to 130.03 ppm in SB-2. In SB-1, for the $\alpha$ carbon of imine linkage, the chemical shift value was found to be at 158.88 ppm, while in SB-2, it was at 158.53 ppm. A chemical shift was observed for the carbon atom that was linked to nitrogen at 149.39 ppm in the case of SB-1 while at 150.17 ppm for SB-2.

*3.2.4. Mass Spectrum (MS).* For validation purposes, mass spectra of the synthesized products were collected, and they are shown in Figure 6a,b. A molecular ion peak at ($m/z$ = 421 for SB-1 and $m/z$ = 479 for SB-2) in the mass spectra of the synthesized Schiff bases was seen, which is consistent with their molecular weights of (420) and (478) for SB-1 and SB-2, respectively, and contributes further support to their structures. There is a strong correlation between the observed peaks of both spectra and the suggested structures of the produced molecules. Additional notable peaks were detected in the SB-1 mass spectrum at $m/z$ values of 65, 75, 89, 178, 195, 287, 302, and 314. Similarly, in the SB-2 mass spectrum, these peaks were identified at $m/z$ values of 65, 75, 89, 178, 224, 313, 331, and 343. These peaks correspond well to the fragments of the synthesized compounds that were proposed, as illustrated in Figure 7a,b. The aforementioned findings provide strong support for the formation of Schiff bases.

**3.3. Scanning Electron Microscopy (SEM).** The SEM technique is electron microscopy that produces meaningful pictures of a material by scanning its surface with a focused electron beam.[47,48] When the electron reacts with the sample atom, it sends out different signals that reveal the surface


https://doi.org/10.1021/acsomega.4c02007
ACS Omega 2024, 9, 35431−35448

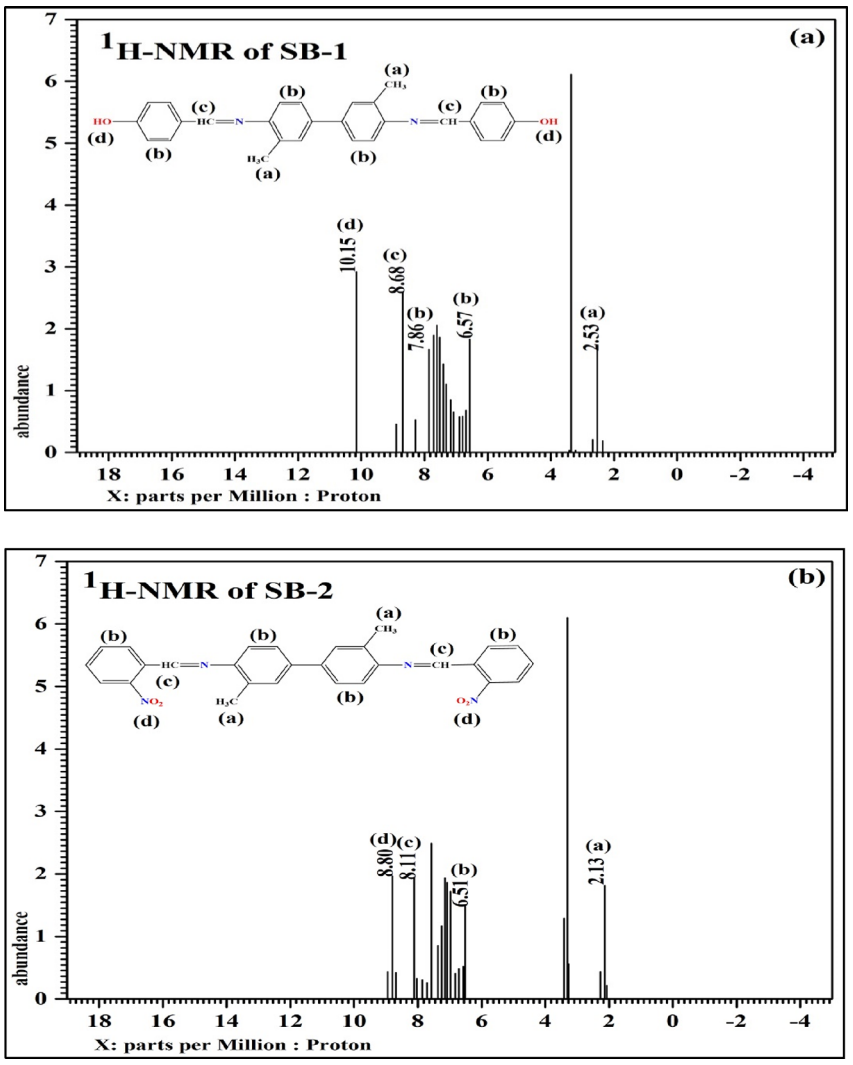


**Figure 4.** (a, b) $^1$H NMR spectrum of Schiff base-1 and Schiff base-2, respectively.

topography, size, and shape of the synthesized compound. In modern materials chemistry, SEM is often used to figure out the shape of a surface. We used our pieces of amorphous powder to perform a SEM experiment. Figure 8a,b shows the different pictures of SB-1 and SB-2. The SEM images showed clearly that the sheets were spread out and overlapped. Figure 8a shows that Schiff base-1 has structures that look like sheets. In the case of Schiff base-2 (Figure 8b), particles that look like rods can be seen.

**3.4. X-ray Diffraction (XRD).** XRD stands as the primary technique for discerning the crystallographic structure and phase of materials. It offers swift analysis, yielding unit cell dimensions, and is chiefly employed for identifying crystalline material phases. The prepared samples underwent assessment using the Rigaku Ultima IV Powder X-ray diffractometer, employing Cu−K$\alpha$ radiation with a wavelength of 1.542 Å (X-ray), to ascertain their structure.[49] The XRD patterns of Schiff base-1 and Schiff base-2 are depicted in Figure 9a,b, respectively. The synthesized compound SB-1 possesses a triclinic crystal structure having lattice parameters $a$ = 8.04 Å, $b$ = 13.55 Å, $c$ = 14.07 Å, $\alpha$ = 68.65°, $\beta$ = 76.41°, and $\gamma$ = 81.65°, while SB-2 possesses a tetragonal crystal structure having lattice parameters $a$ = 10.40 Å, $b$ = 10.40 Å, $c$ = 8.50 Å, $\alpha$ = 90°, $\beta$ = 90°, and $\gamma$ = 90°.[49] The most prominent peak observed for SB-1 is at $2\theta$ = 17.36° (1 2 2). The most prominent peak observed for SB-2 is at 17.22° (200).

The XRD spectrum reveals the polycrystalline nature of the synthesized material. The presence of minor peaks in the XRD pattern states decreases in degree of crystallization. The decrease in the degree of crystallization deteriorates the attributes of the material. The attributes change at the grain boundary of the polycrystal, making the material behavior anisotropic. For SB-1, the most significant peak found is at $2\theta$ = 17.360 (1 2 2), while the most prominent peak observed for SB-2 is at $2\theta$ = 17.22° (200). The XRD parameters are shown in Tables 2 and 3 for SB-1 and SB-2, respectively.

To forecast the average size of a sample's crystallites (in nanometers), Scherrer's relation is used.[50,51]

$$D = \frac{k\lambda}{\beta_{hkl}\cos\theta} \tag{4}$$

In this case, the X-ray wavelength is represented by $\lambda$, and the shape constant $k$ is given a value of 0.95 for organic molecules. The full-width at half-maximum (fwhm) of diffraction peaks or planes is represented by $\beta_{hkl}$, while the diffraction angle is indicated by $\theta$. For SB-1 and SB-2, the calculated values for $D$ are found to be 24.64 and 28.59 nm, respectively.


https://doi.org/10.1021/acsomega.4c02007
ACS Omega 2024, 9, 35431−35448

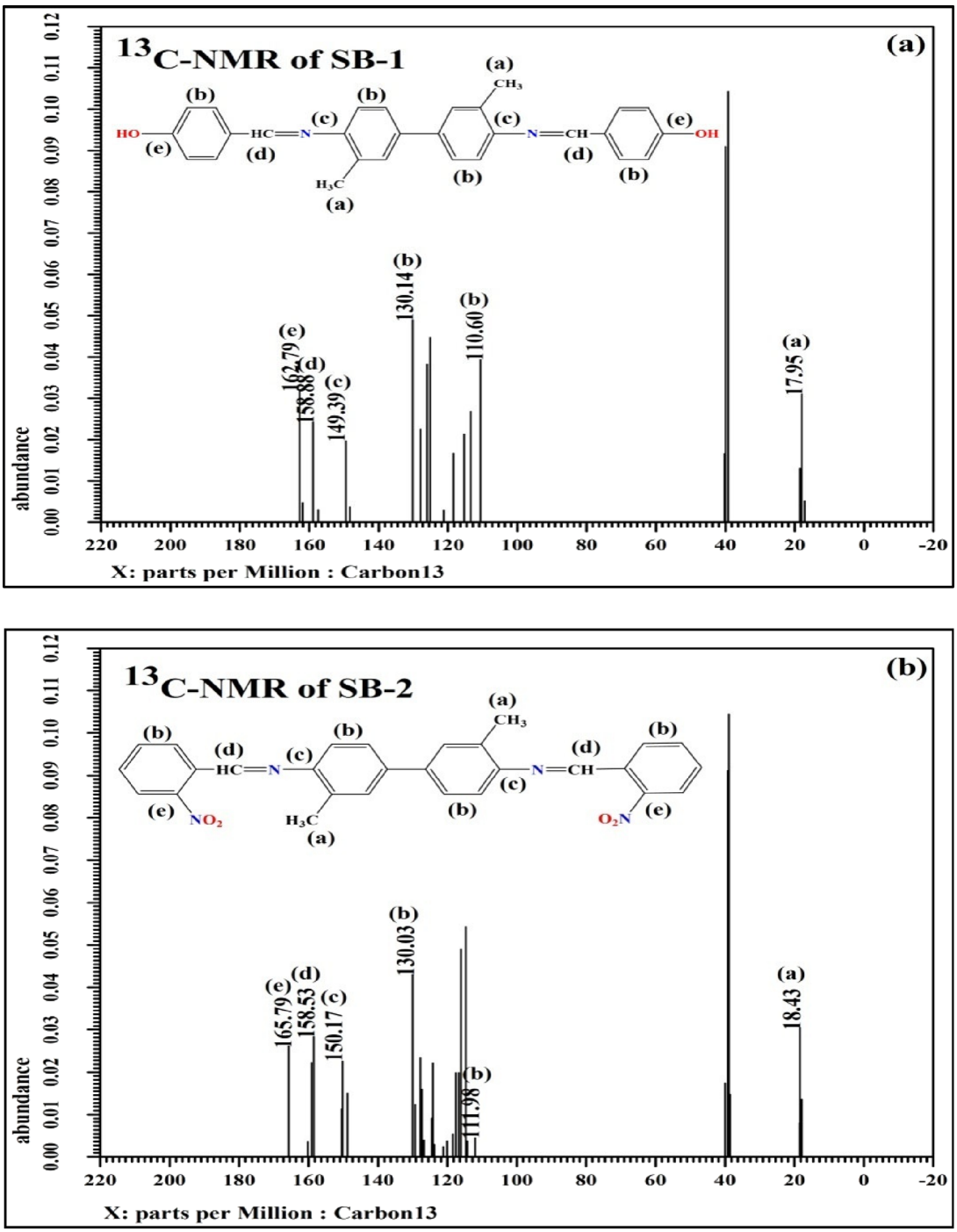


**Figure 5.** (a, b) $^{13}$C NMR spectrum of Schiff base-1 and Schiff base-2, respectively.

In addition, the dislocation density is determined for the as-synthesized compounds. The dislocation density values are found to be $1.68 \times 10^{15}$ and $1.22 \times 10^{15}$ m$^{-2}$ for SB-1 and SB-2, respectively. The dislocation density is estimated through the following relation.[52−54]

$$\delta = \frac{1}{D_{\mathrm{XRD}}{}^{2}} \tag{5}$$

Dislocation density in the unit area line is represented by $\delta$.

**3.5. Thermal Study.** For Schiff base-1 and Schiff base-2, the TG, DTA, and DTG thermocurves are measured concurrently (Figure 10a−c for SB-1, while Figure 11a−c for SB-2). Thermodynamic curves are recorded in a nitrogen-free chamber at 10, 15, and 20 K·min$^{-1}$ heating rates, with temperatures ranging from ambient to 430 K. The TG curves in Figures 10a and 11a demonstrate a correlation between the heating rates and a constant weight loss in the sample. Figures 10b and 11b show the simultaneous DTA curves, which show an initial endothermic phase followed by an exothermic transition. The first endothermic behavior suggests that both hydrous and loosely linked groups absorb heat, which results in their loss.[55] Analysis from the TG curves indicates decomposition of the sample at higher temperatures, with a subsequent exothermic character evident later in the process,


https://doi.org/10.1021/acsomega.4c02007
ACS Omega 2024, 9, 35431−35448

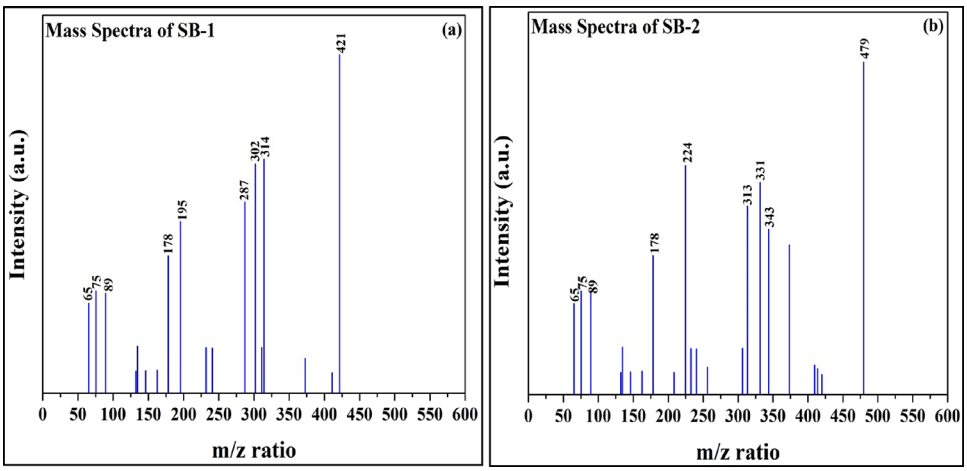


**Figure 6.** (a, b) Mass spectra of SB-1 and SB-2, respectively.

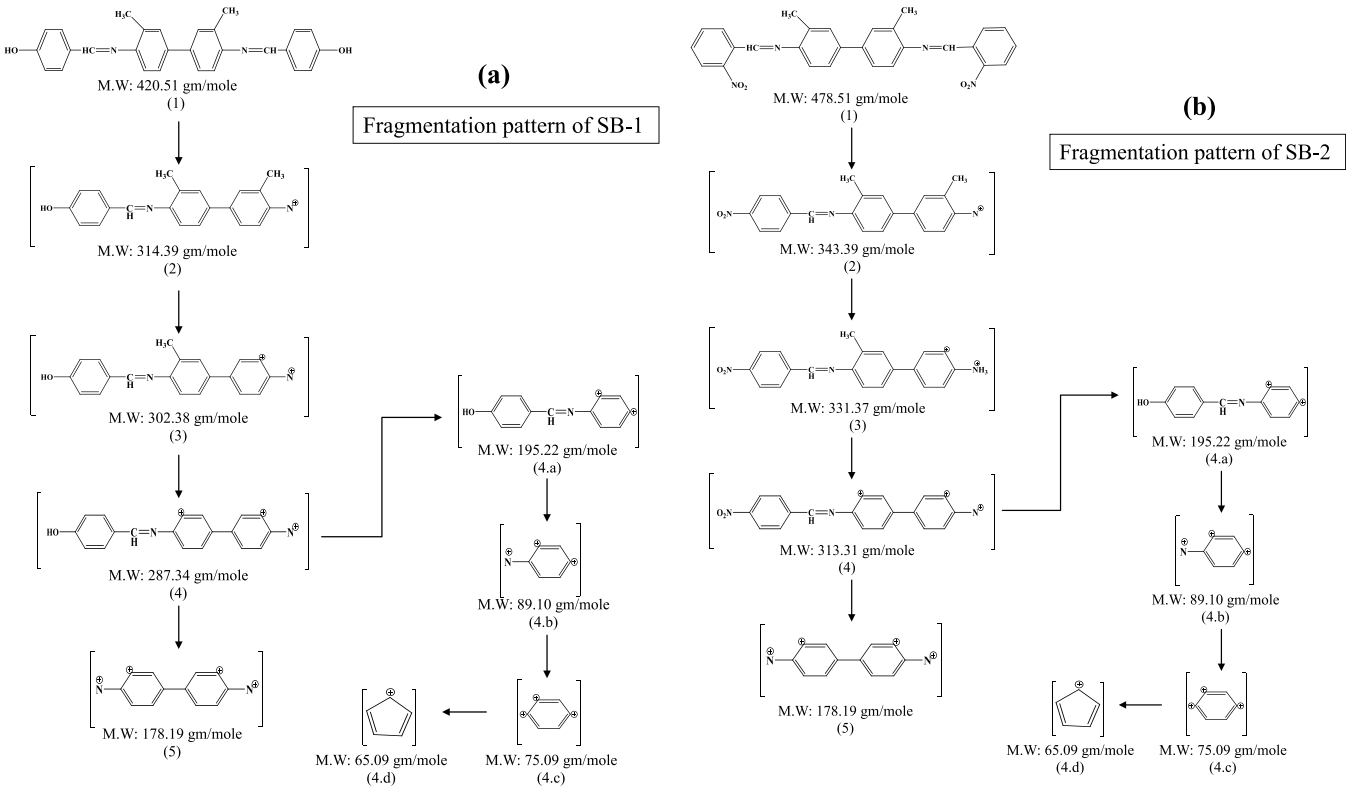


**Figure 7.** (a, b) Proposed mass fragmentation pattern of SB-1 and SB-2, respectively.

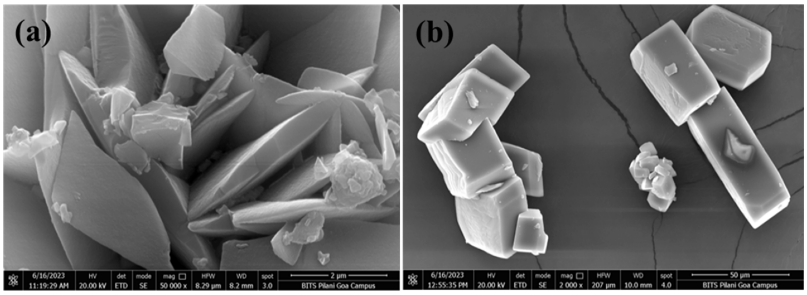


**Figure 8.** (a, b) SEM Images of Schiff base-1 and Schiff base-2, respectively.

as shown in Figures 10a and 11a. Figures 10c and 11c show the unique and solitary decomposition peaks in the DTG thermal curves, which are used to derive kinetic parameters. The thermal decomposition of the sample with a rise in



https://doi.org/10.1021/acsomega.4c02007
ACS Omega 2024, 9, 35431−35448

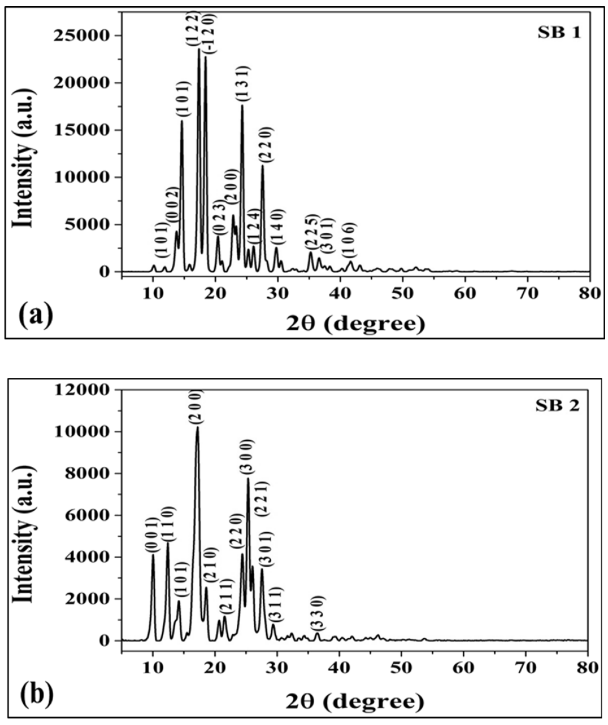


**Figure 9.** XRD patterns of (a) SB-1 and (b) SB-2.

**Table 2. XRD Parameters of the Schiff Base-1-Derived Product**

| (*hkl*) | 2*θ* | *d* (Å) | intensity (a.u.) |
|---|---|---|---|
| (101) | 11.90 | 8.71 | 523 |
| (002) | 13.78 | 7.42 | 4300 |
| (−101) | 14.62 | 6.42 | 16,022 |
| (122) | 17.36 | 5.58 | 23,660 |
| (−120) | 18.41 | 5.10 | 22,804 |
| (023) | 20.41 | 4.81 | 3787 |
| (200) | 22.84 | 4.21 | 6013 |
| (131) | 24.28 | 3.81 | 17,689 |
| (124) | 26.10 | 3.52 | 2727 |
| (220) | 27.54 | 3.41 | 11,271 |
| (140) | 29.74 | 3.16 | 2570 |
| (225) | 35.24 | 2.72 | 2080 |
| (301) | 36.59 | 2.54 | 1475 |
| (101) | 11.90 | 8.71 | 523 |

temperature means that the temperature increase causes the breakdown of order in the sample and disrupts the attributes of the samples. Also, the interaction between the components increases with heating rate.[56]

The weight loss percentages for each heating rate are shown in Table 4.

Table 4 clearly reveals that the weight loss of SB-1 is more than that of SB-2 due to analysis at comparatively higher temperature. The increased weight loss can be ascribed to the uneven heating of the samples, resulting in a more random heating process. There is further breakdown of the material as a result of this uneven heating. The DTA thermocurves first exhibit endothermic activity when hydrated materials are present. Then, exothermic activity is visible when the sample decomposes.

**3.6. Kinetic Analysis.** Kinetic parameters are estimated using isoconversional linear approaches such as Friedman

**Table 3. XRD Parameters of the Schiff Base-2-Derived Product**

| (*hkl*) | 2*θ* | *d* (Å) | intensity (a.u.) |
|---|---|---|---|
| (001) | 10.05 | 8.50 | 4129 |
| (110) | 12.43 | 7.35 | 4710 |
| (101) | 13.76 | 6.58 | 973 |
| (200) | 17.22 | 5.20 | 10,244 |
| (210) | 18.60 | 4.65 | 2551 |
| (211) | 21.55 | 4.08 | 1171 |
| (220) | 24.40 | 3.67 | 4154 |
| (300) | 25.32 | 3.46 | 7798 |
| (221) | 26.04 | 3.37 | 3589 |
| (301) | 27.55 | 3.20 | 3436 |
| (311) | 29.34 | 3.06 | 785 |
| (330) | 36.47 | 2.45 | 371 |
| (001) | 10.05 | 8.50 | 4129 |
| (110) | 12.43 | 7.35 | 4710 |

(FR), Flynn−Wall−Ozawa (FWO), and Kissinger−Akahira−Sunose (KAS). FR is a differential method, whereas KAS and FWO are integral procedures. With an isoconversional approach, these approaches are most commonly employed in non-isothermal kinetic research.

*3.6.1. KAS Method.* The Coats−Redfern (CR) estimate[57,58] is the foundation of the integral KAS technique.[59] Using this approach, we use the formula

$$\ln\left(\frac{\beta}{T^2}\right) = \ln\left(\frac{AR}{E_a f(\alpha)}\right) - \frac{E_a}{RT} \quad (6)$$

The heating rate, activation energy, phonon frequency factor, absolute temperature where DTG peaks occur, integral transform function, and universal gas constant are indicated by variables $\beta$, $E_a$, $A$, $T$, $f(\alpha)$, and $R$ in this equation. The phonon frequency factor is a pre-exponential Arrhenius factor arising due to the thermally activated lattice vibration. The lattice vibrations are of finite frequency depending on the sample's crystal structure.[60]

The KAS plot of the sample with a single decomposition peak is shown in Figure 12a,b.

With a given $\alpha$ value, a linear connection is obtained when plotting $\ln(\beta/T^2)$ versus 1/T. Indicators of the activation energy ($E_a/R$) and $\ln(AR/E_a f(\alpha))$, respectively, are the slope and intercept of this line. When calculating kinetic parameters such as the activation energy ($E_a$) and phonon frequency factor (A), the values of the slope and intercept are very helpful.

$$E_a = -(\text{slope}\cdot R) \quad (7)$$

$$A = \frac{E_a \cdot \exp.(\text{intercept})}{R} \quad (8)$$

*3.6.2. FWO Method.* The integral FWO technique is predicated on the following equation[61,62]:

$$\ln \beta = -1.052\left(\frac{E_a}{RT}\right) + \ln\left(\frac{AE_a}{R}\right) - \ln(f(\alpha)) - 5.33 \quad (9)$$

As in the KAS technique, each term in this equation has the same meaning.

The FWO plot of the sample with a single decomposition peak is shown in Figure 13a,b.

Plotting $\ln \beta$ versus $1/T$ yields a straight line with a constant $\alpha$ value. The intercept and slope of the straight line are,


https://doi.org/10.1021/acsomega.4c02007
ACS Omega 2024, 9, 35431−35448

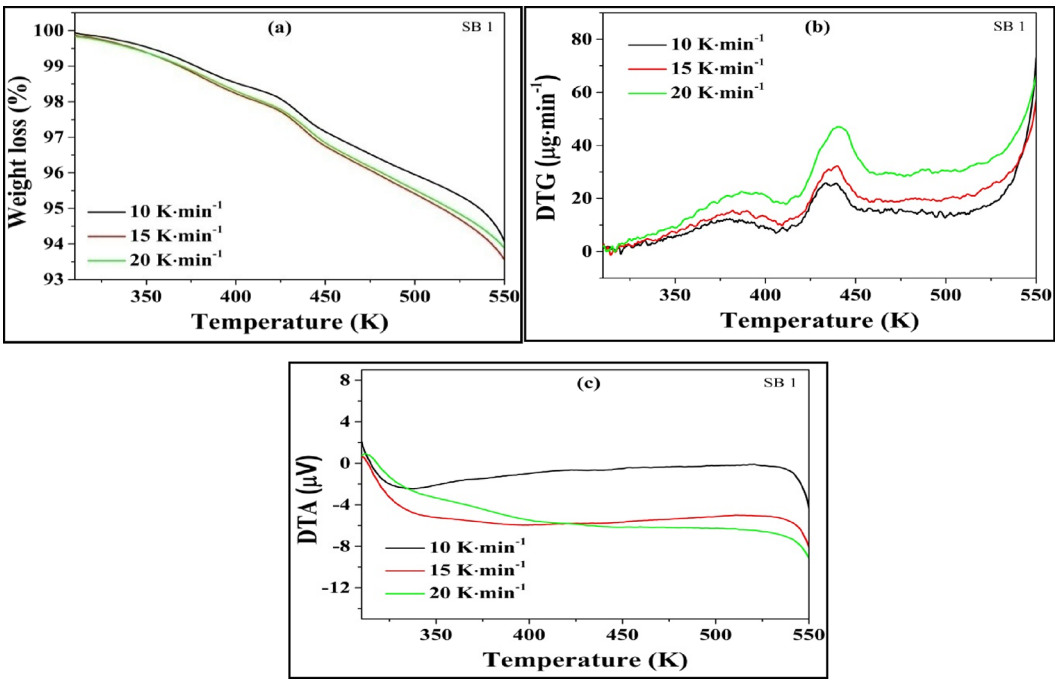


**Figure 10.** (a) TG, (b) DTG, and (c) DTA curves for SB-1 in a nitrogen atmosphere.

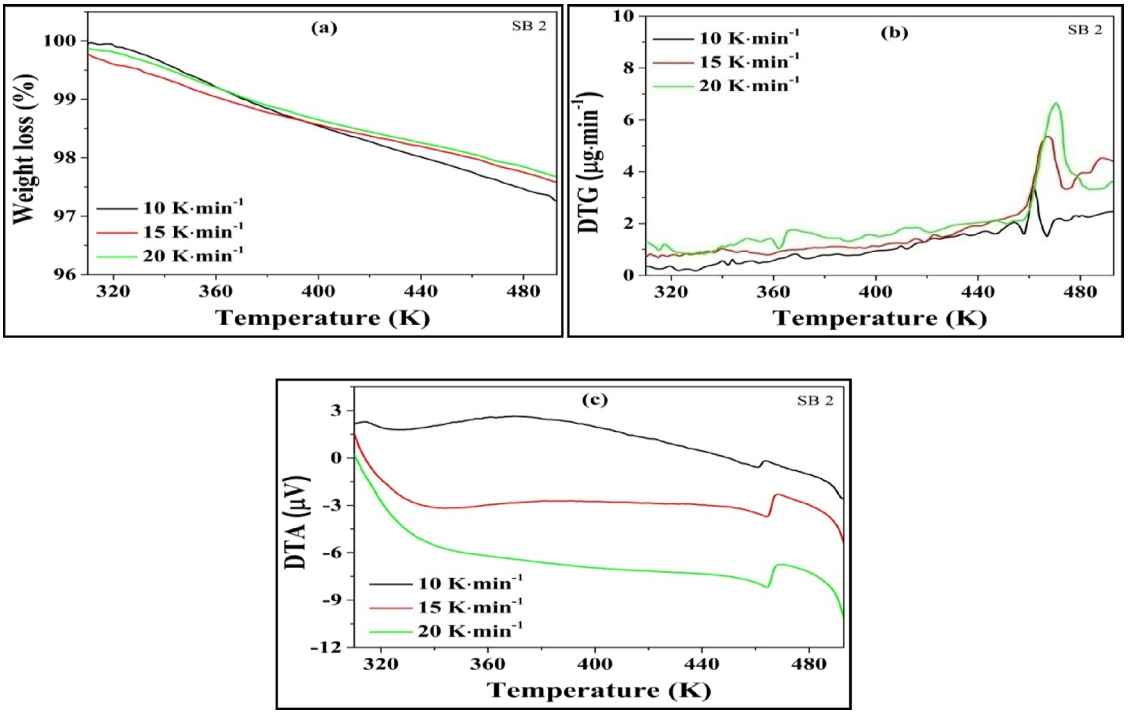


**Figure 11.** (a) TG, (b) DTG, and (c) DTA curves for SB-2 in a nitrogen atmosphere.

**Table 4. Temperature Range and Observed Weight Loss of the Sample**

| | weight loss (%) | |
|---|---|---|
| heating rate (K·min$^{-1}$) | **SB-1**, 308−550 K | **SB-2**, 308−490 K |
| 10 | 5.89 | 2.75 |
| 15 | 6.38 | 2.41 |
| 20 | 6.09 | 2.33 |

respectively, $\ln(AE_a/R)$ and $1.052(E_a/R)$. When calculating kinetic parameters like activation energy ($E_a$) and phonon frequency factor ($A$), the slope and intercept are helpful:

$$E_a = -\left(\frac{\text{slope}\cdot R}{1.052}\right) \tag{10}$$

$$A = \frac{R\cdot\exp.(\text{intercept})}{E_a} \tag{11}$$



https://doi.org/10.1021/acsomega.4c02007
ACS Omega 2024, 9, 35431−35448

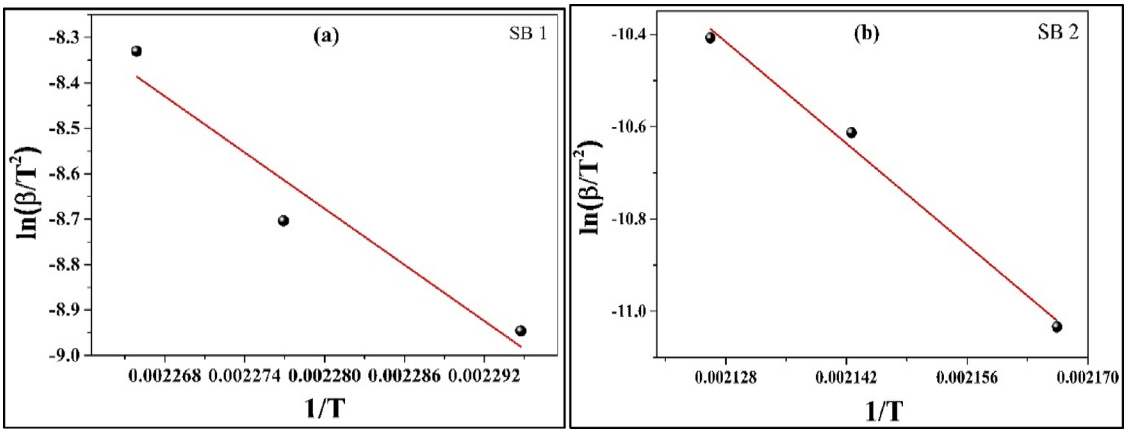


**Figure 12.** (a, b) KAS plot of SB-1 and SB-2, respectively.

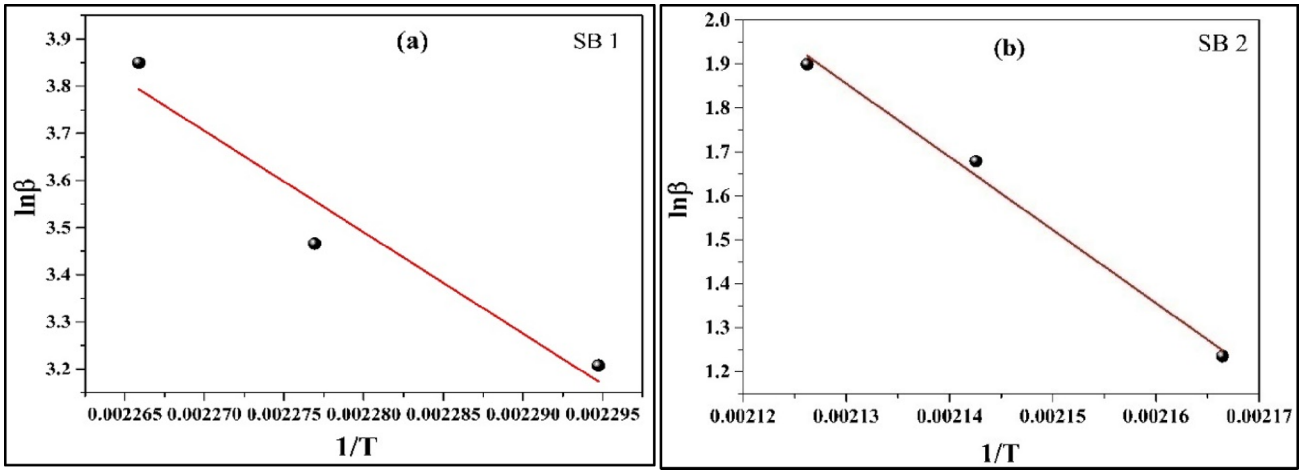


**Figure 13.** (a, b) FWO plot of SB-1 and SB-2, respectively.

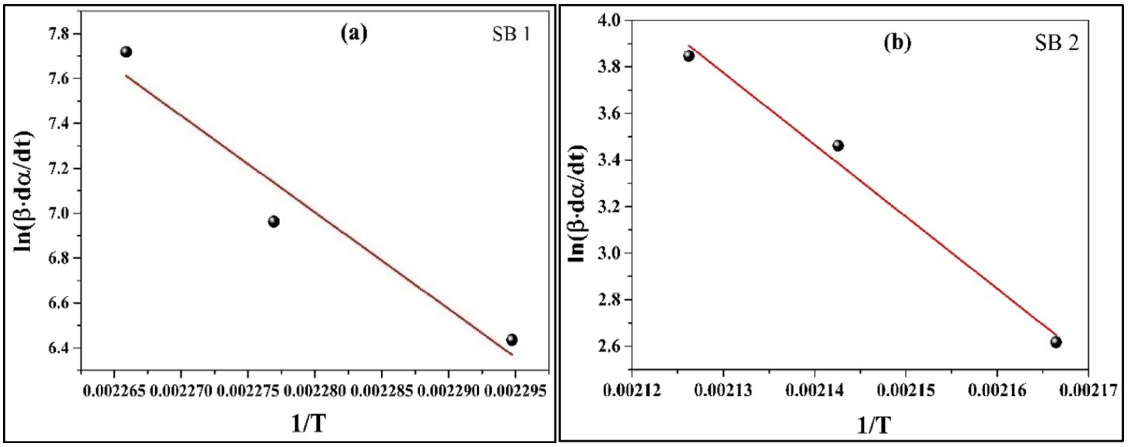


**Figure 14.** (a, b) FR plots of SB-1 and SB-2, respectively.

*3.6.3. FR Method.* This following equation serves as the foundation for the differential FR technique[63]:

$$\ln\left(\beta\frac{d\alpha}{dt}\right) = \ln(A\cdot f(\alpha)) - \frac{E_a}{RT} \quad (12)$$

The FR plot of the sample with a single decomposition peak is displayed in Figure 14a,b.

In this instance, $d\alpha/dt$ represents the differential rate of change in the degree of decomposition. When $\ln(\beta\cdot d\alpha/dt)$ is plotted against $1/T$, the existence of a linear relationship may be shown by keeping $\alpha$ constant. The intercept and slope of the fitted line are $\ln(A\cdot f(\alpha))$ and $-(E_a/R)$, respectively. With these slope and intercept values, kinetic parameters such as activation energy ($E_a$) and phonon frequency factor ($A$) may be computed:

$$E_a = -(\text{slope}\cdot R) \quad (13)$$



https://doi.org/10.1021/acsomega.4c02007
ACS Omega 2024, 9, 35431−35448

Table 5. Thermodynamic Parameters of Schiff Base Compounds

| sample | method | $E_a$(kJ·mol$^{-1}$) | $A$ (s$^{-1}$) | $\Delta S^*$(J·K$^{-1}$·mol$^{-1}$) | $\Delta H^*$(kJ·mol$^{-1}$) | $\Delta G^*$(kJ·mol$^{-1}$) |
|---|---|---|---|---|---|---|
| SB-1 | KAS | 177.44 | $9.13 \times 10^{20}$ | 153.22 | 167.79 | 100.56 |
| | FWO | 169.89 | $3.11 \times 10^{18}$ | 105.92 | 166.25 | 119.77 |
| | FR | 178.98 | $1.35 \times 10^{16}$ | 60.68 | 175.33 | 148.71 |
| SB-2 | KAS | 130.66 | $1.57 \times 10^{14}$ | 23.14 | 126.78 | 115.99 |
| | FWO | 131.56 | $1.01 \times 10^{12}$ | 18.82 | 127.68 | 118.91 |
| | FR | 128.38 | $1.27 \times 10^{10}$ | 55.21 | 124.51 | 98.76 |

$$A = \frac{\exp.(\text{intercept})}{f(\alpha)} \tag{14}$$

The values of activation energy ($E_a$) and phonon frequency factor ($A$) determined by these three methods are tabulated in Table 5.

*3.6.4. Thermodynamic Parameters.* The determined $E_a$ and $A$ values from KAS, FWO, and FR methods were used to derive the change in activation enthalpy ($\Delta H^*$), entropy ($\Delta S^*$), and Gibb's free energy ($\Delta G^*$)[64]:

$$\Delta H^* = E_a - RT \tag{15}$$

$$\Delta S^* = R \cdot \ln\left(\frac{Ah}{k_B T}\right) \tag{16}$$

$$\Delta G^* = \Delta H^* - T\Delta S^* \tag{17}$$

The expected values for $E_a$, A, $\Delta H^*$, $\Delta S^*$, and $\Delta G^*$ can be seen in Table 5.

Table 5 shows the dynamic values that were found using the three different methods. This result shows that the predictions made by the three temperature methods are correct.

It is clear that heat absorption leads to decomposition since the $\Delta H^*$ values are positive. The disorder level increases when the value of $\Delta S^*$ is positive. The presence of positive $\Delta G^*$ values suggests that decomposition did not occur naturally. The gradual and constant rise in the temperature is responsible for this degradation.

**3.7. Biological Activities.** *3.7.1. Antidiabetic Activity Using α-Amylase Inhibition Assay.* The primary method for assessing the produced compounds' antidiabetic efficacy was the inhibition of α-amylase, with comparisons made to the conventional drug acarbose, which displayed 80.80% inhibition. As shown in the data in Table 6, SB-2 surpassed both SB-1 and the standard acarbose in terms of efficacy. With an inhibition level of 86.7%, SB-2 demonstrated the highest level of α-amylase inhibition. All of the structural elements of Schiff bases, especially the phenyl ring with different substituents and imine functionality present in both molecules, have contributed to this increased inhibitory effect. Both compounds share two important structural elements: phenyl rings and imine functionality. Table 6 represents α-amylase inhibition by synthetic compounds and the standard.

Table 6. α-Amylase Inhibition of Schiff Bases and Standard Acarbose

| compound name | % α-amylase inhibition |
|---|---|
| SB-1 | 81.9 |
| SB-2 | 86.7 |
| acarbose standard | 80.8 |

*3.7.2. Kinetic Study of α-Amylase Inhibition Assay.* As shown in Figure 15, Schiff base-1 and Schiff base-2 were chosen to examine kinetic investigations based on their inhibition, ranging from 86.7 to 81.9%. Due to this, different concentrations of the substrate starch (concentration: 30 mM; aliquots: 0.1−1 mL) and the inhibitor (concentration: 1 mg/mL; aliquots: 0.5 mL) were utilized.

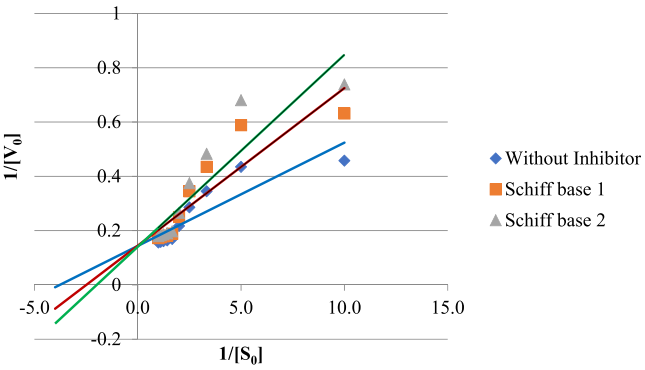


**Figure 15.** Lineweaver−Burk plots of reciprocal of the substrate against reciprocal of the rate of reaction showing the effect of competitive inhibition at fixed enzyme concentration.

Lineweaver−Burk plots were used to identify the different types of α-amylase inhibitors. The reciprocal of the substrate [$S_0$] was plotted against the reciprocal of the reaction rate [$V_0$] to assess the impact of the inhibitors, or Schiff bases, on $V_{max}$ and $K_m$ values. With the inhibitor, the values of $K_m$ and $V_{max}$ fell between 0.4 and 0.5 M/min/mL and 6.9 mM, respectively. Similarly, $K_m$ was 0.27 M/min/mL and $V_{max}$ was 6.9 M without the inhibitor. Thus, it was determined that only the $K_m$ value had changed; the $V_{max}$ value remained unchanged. Thus, there was no influence on $V_{max}$ and a competitive kind of inhibition was indicated by the rising value of $K_m$ for both Schiff bases.

*3.7.3. Antidiabetic Activity by Using Molecular Docking Study.* Molecular docking investigations were undertaken to predict how Schiff bases bind to pancreatic α-amylase and to explore their specific intermolecular interactions. The wild type of human pancreatic amylase (PDB ID: 4X9Y) was docked with Schiff bases as well as the standard inhibitor, acarbose. Here, Figure 16a demonstrates the interactions of Schiff base-1 with the active sites of receptor (4X9Y) in a 2D schematic. Likewise, Figure 16b displays the interactions of Schiff base-2 with the same receptor. Additionally, Figure 16c exhibits the interactions of standard acarbose with the receptor's active sites in 2D schematics.

Table 7 outlines the docking scores (binding energy).

Compared to acarbose, which had a binding energy of −7.50 kcal/mol, Schiff bases exhibited more favorable binding energies of 9.0 and −9.5 kcal/mol. Using Discovery Studio


https://doi.org/10.1021/acsomega.4c02007
ACS Omega 2024, 9, 35431−35448

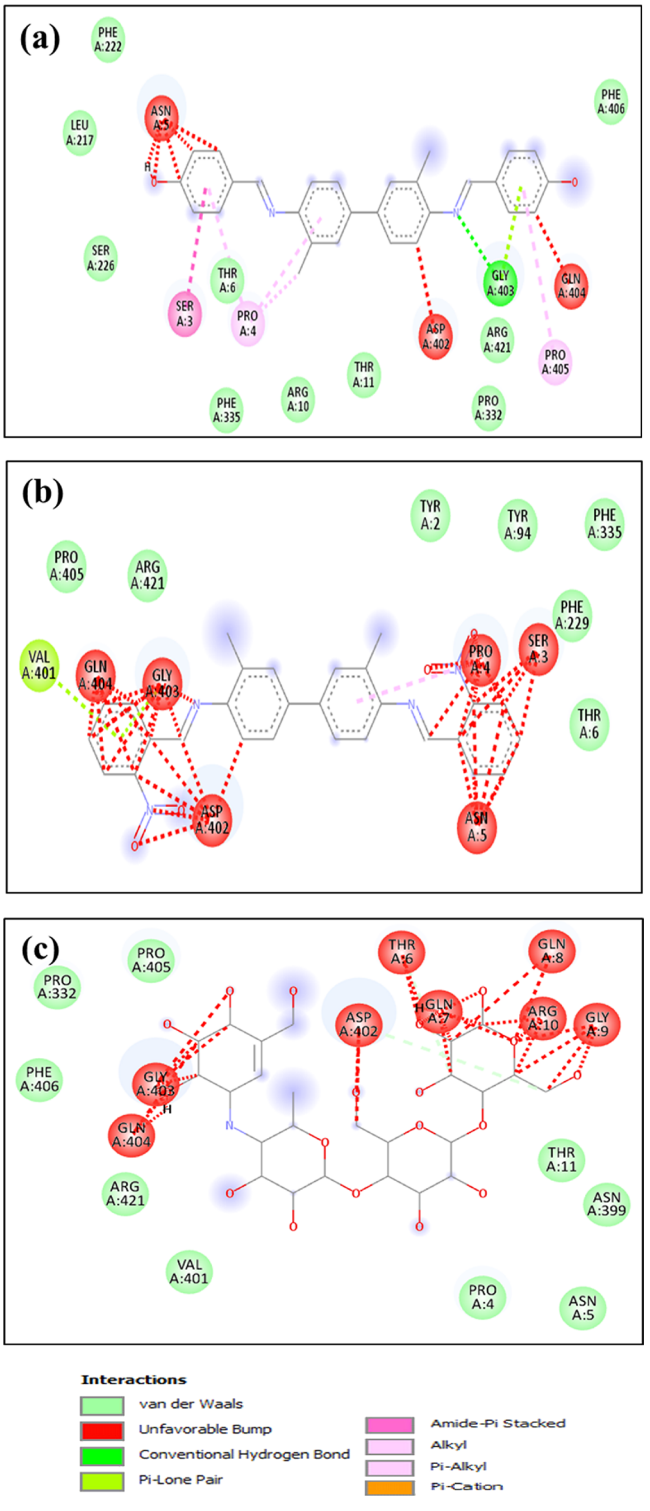


**Figure 16.** (a−c) Interaction of SB-1, SB-2, and standard acarbose, respectively, with the active sites of receptor (4X9Y) in a 2D schematic.

**Table 7. Binding Energy of Schiff Bases and Standard Acarbose**

| compound name | binding energy (kcal/mol) |
|---|---|
| SB-1 | −9.0 |
| SB-2 | −9.5 |
| acarbose standard | −7.5 |

4.5, the binding mechanisms of acarbose and Schiff bases to the receptors were investigated.

**3.8. *In Vitro* Cytotoxicity Study.** *3.8.1. In Vitro Cytotoxicity Study by Using Human Lung Cancer Cell Line A549.* Following 24 h of treatment, the concentrations of Schiff base compounds that result in a 50% suppression of the A549 cell line's viability are highlighted in the data (Figure 17). SB-1 demonstrated an $IC_{50}$ value of 139.1 ± 0.433 μg/mL, while SB-2 exhibited a value of 359.5 ± 0.867 μg/mL against A549 cells. On the other hand, the $IC_{50}$ value on A549 cells was 10.20 ± 1.82 μg/mL for the conventional medicine Methotrexate. These results suggest that Schiff bases possess significant cytotoxicity to A549 cells. Notably, SB-1 displayed a lower $IC_{50}$ value compared to SB-2, indicating its superior anticancer efficacy.

*3.8.2. In Vitro Cytotoxicity Studies by Using C. elegans.* Elevated levels of oxidative stress have been identified as a significant contributor to the aging process and age-related diseases. An evaluation of stress resistance and anti-Alzheimer's properties of synthetic compounds has been done on *C. elegans* in the present study.

*3.8.2.1. Evaluation of $LD_{50}$ of Synthesized Schiff Bases.* *C. elegans* has been proved an effective model for toxicity studies as it helps to predict the toxicity in mammals.[65] $LD_{50}$ was determined using the concentration of synthetic compounds in the range of 10−100 μg/mL, and counts of dead worms were kept until every last one had died. The concentration at which 50% of the worms died was considered as $LD_{50}$ of respective compounds. The effect of various synthetic compounds was explored in *C. elegans* by the addition of compounds along with NGM agar at a dose according to 1/10th $LD_{50}$ values. Figure 18a,b depicts the percentage of dead worms against the concentration of compounds. The value of $R^2$ and the slope equation are displayed within each graph.

Using these graphs, the $LD_{50}$ can be determined by applying a slope equation (Table 8). The determined $LD_{50}$ can be used to finalize the concentration of compounds for further experiments. The value that is 1/10th of the $LD_{50}$ was used for the remaining experiments.

*3.8.2.2. Stress-Resistant Properties of Synthetic Compounds in C. elegans.* Additionally, the compounds' impact under stress circumstances was assessed. The tests for thermal and oxidative stress resistance were conducted to examine the worms' ability to withstand stress in response to certain chemicals.

*3.8.2.3. Thermal Assay.* To evaluate the impact of compounds on *C. elegans* survival at elevated temperatures, a thermal experiment was conducted. To lessen the heat stress, the extract-treated and control synchronized worms were transferred from 20 to 35 °C. Up to the 12th hour, the dead worms were counted every 2 h, and the mean survival was calculated using those data.

The mean survival of treated worms was higher than that of untreated worms according to the data. Worms treated with SB-2 had the highest mean survival rate (Table 9).

*3.8.2.4. Oxidative Stress Assay.* Another stress resistance assay was performed to check the capacity of worms to fight against elevated levels of oxidative stress. Soaking the synchronized worms in a hydrogen peroxide (20 mM) solution for 2 h caused oxidative stress in both the treatment and control groups. After that, the worms were moved to a fresh NGM plate and kept in an incubator at 20 °C for 16 h. The live worms were counted after completion of 16 h. As the


https://doi.org/10.1021/acsomega.4c02007
ACS Omega 2024, 9, 35431−35448

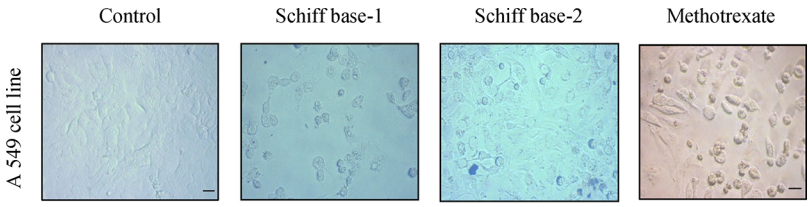


**Figure 17.** Morphological changes induced by Schiff bases and Methotrexate standard drug on A549 cell lines.

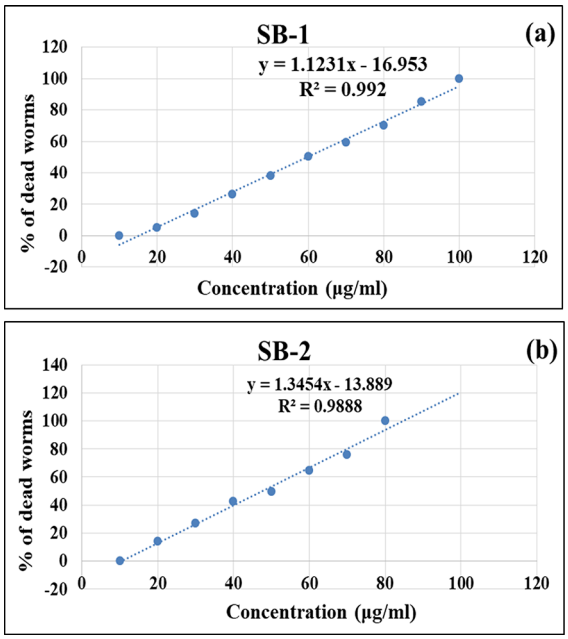


**Figure 18.** (a, b) Percentage of dead worms against SB-1 and SB-2, respectively.

**Table 8. $LD_{50}$ Values of Each Schiff Base Compound**

| compound name | $LD_{50}$ | 1/10th of $LD_{50}$ |
|---|---|---|
| SB-1 | 59.77 $\mu$g/mL | 5.9 $\mu$g/mL |
| SB-2 | 47.67 $\mu$g/mL | 4.76 $\mu$g/mL |

**Table 9. Mean Survival Rate of Treated and Control Worms under Thermal Stress**

| compound name | mean life span (h) |
|---|---|
| PC | 9.333333 |
| NC | 9.233333 |
| SB-1 | 11.36667 |
| SB-2 | 11.6 |

results showed, worms treated with compounds survived more than did control worms.

In comparison with the other extracts, the worms that were treated with SB-2 exhibited the highest survival rate (Table 10). Research has demonstrated that a reduction in oxidative stress is additionally associated with a decrease in age-related maladies.

*3.8.2.5. Influence of Synthetic Compounds on Mitigating Paralysis Induced by Amyloid-$\beta$ Expression.* Synthetic compounds were further applied to *C. elegans* to check its therapeutic potential against diseases. It was analyzed using the transgenic *C. elegans* CL4176, which is engineered to express the human amyloid-$\beta$ protein (A$\beta$) upon upshifting to a higher temperature. When the temperature was increased from 16 to 25 °C, the induction of amyloid-$\beta$ protein synthesis in the *C. elegans* muscle cells led to paralysis in both the treated and control worms. Every 2 h, the number of paralyzed worms was counted, and the proportion of paralyzed worms was plotted against time on a graph.

**Table 10. Percentage Survival of Worms under Oxidative Stress**

| compound name | percentage survival |
|---|---|
| PC | 32.22 |
| NC | 37.77 |
| SB-1 | 75.55 |
| SB-2 | 67.77 |

The study's findings indicated that the treated worms had delayed paralysis compared to the control worms (Figure 19). Worms fed Schiff bases exhibited the longest period of paralysis delay.

## 4. SAR STUDIES (STRUCTURE–ACTIVITY RELATIONSHIP)

In the exploration of molecular docking, the binding models indicate that the synthesized compounds are bound in the active site via a variety of hydrogen bonding interactions.

Both compounds had high binding energies as compared to those of standard acarbose. SB-2 showed the highest binding energy (−9.5 kcal/mol). In the evaluation of antidiabetic activity by $\alpha$-amylase inhibition assay, both compounds were found more potent than standard acarbose, and among them, SB-2 showed the highest inhibition of 86.7% than SB-1 (81.9%) and standard (80.8%). This may be due to the presence of methyl, nitro, and hydroxy groups in the aromatic ring. The human lung cancer cell line A549 was used to assess the *in vitro* cytotoxicity of the resultant complexes. Different substituent groups in the salicyl ring in the Schiff bases suggest various levels of cytotoxicity. The results show that SB-1 ($IC_{50}$ = 139.1 ± 0.433 $\mu$g/mL) has superior cytotoxicity compared to SB-2 ($IC_{50}$ = 359.5 ± 0.867 $\mu$g/mL).

Although both the compounds possess the same fundamental structure, research into the relationship between their structure and bioactivity shows that the various phenyl ring substituents have a significant impact on both the compounds' biological and physical characteristics.

## 5. CONCLUSIONS

A new, environmentally friendly, and safe method was employed to synthesize Schiff bases utilizing lemon juice as a catalyst. This method operates under moderate reaction conditions and requires a relatively simple experimental setup to achieve satisfactory results. XRD analysis revealed that SB-1 has a triclinic structure, whereas SB-2 exhibits a tetragonal crystal structure. Based on Scherrer's formula applied to the XRD data, the estimated sizes of the SB-1 and


https://doi.org/10.1021/acsomega.4c02007
ACS Omega 2024, 9, 35431−35448

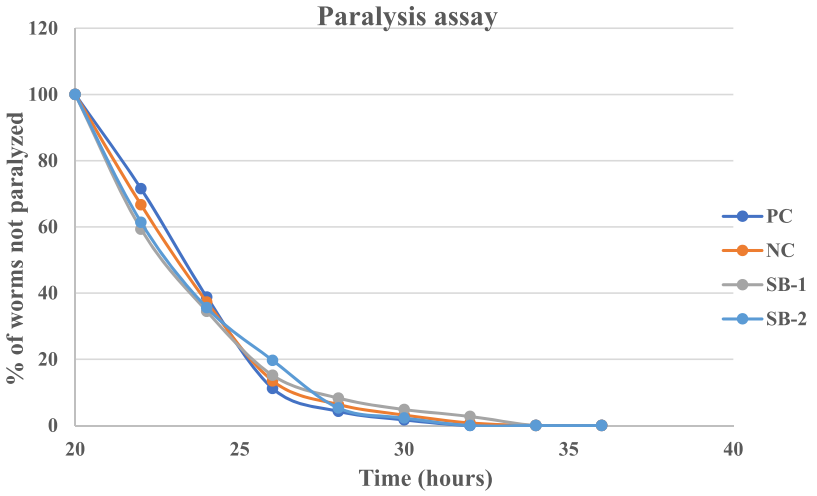


**Figure 19.** Percentage of dead worms against SB-2.

SB-2 crystallites are 24.64 and 28.59 nm, respectively. FTIR, $^{1}$H NMR, and $^{13}$C NMR spectroscopies verified the presence of $\nu$(C═N). TG thermocurves were measured in a nitrogen environment using three different heating rates (10, 15, and 20 K·min$^{-1}$) over two temperature ranges: 308 to 550 K for SB-1 and 308 to 490 K for SB-2. Initially, the DTA thermocurves displayed endothermic activity due to the loss of hydrated samples, transitioning to exothermic behavior as the sample underwent decomposition. Kinetic parameters were estimated using the KAS, FWO, and FR techniques. SEM analysis revealed that the SB-1 molecule has a sheet-like form, whereas the SB-2 molecule has a rod-like structure. The compounds' *in vitro* activity against diabetes was examined. By inhibiting $\alpha$-amylase enzymes, these substances' antidiabetic research may lower the blood's postprandial glucose level, which can be a crucial tactic in controlling blood sugar. Schiff base-1 and Schiff base-2 both exhibited potent cytotoxic effects on the A549 human lung cancer cell line, with corresponding $IC_{50}$ values of 139.1 ± 0.433 and 359.5 ± 0.867 $\mu$g/mL, respectively. Also, in the case of *C. elegans* exposed to Schiff bases, they demonstrated the highest survival rate among tested extracts, suggesting their potential in combating oxidative stress and age-related illnesses. Additionally, these compounds delayed paralysis in treated worms compared with controls, underscoring their beneficial properties. The findings clearly suggest that these substances hold potential for use in the food and pharmaceutical industries.

## AUTHOR INFORMATION


### Corresponding Author

**Jatin D. Patel** − *Department of Chemistry, Shri Alpesh N. Patel Post Graduate Institute of Science and Research, Anand, Gujarat 388001, India;* orcid.org/0000-0001-8311-9522; Phone: +919825355242; Email: jdpatel_pri@sanppgi.ac.in

### Authors

**Priteshkumar M. Thakor** − *Department of Chemistry, Shri Alpesh N. Patel Post Graduate Institute of Science and Research, Anand, Gujarat 388001, India;* orcid.org/0000-0002-6121-2168

**Rajesh J. Patel** − *Department of Chemistry, Sardar Patel University, Anand, Gujarat 388001, India*

**Sunil H. Chaki** − *Department of Physics, Sardar Patel University, Anand, Gujarat 388001, India*

**Ankurkumar J. Khimani** − *Department of Physics, Shri Alpesh N. Patel Cnce and Research, Anand, Gujarat 388001, India*

**Yati H. Vaidya** − *Department of Microbiology, Shri Alpesh N. Patel Post Graduate Institute of Science and Research, Anand, Gujarat 388001, India*

**Anita P. Chauhan** − *Department of Biotechnology, Shri Alpesh N. Patel Post Graduate Institute of Science and Research, Anand, Gujarat 388001, India*

**Amit B. Dholakia** − *School of Science, Birsa Munda Tribal University, Rajpipla, Gujarat 393145, India*

**Vishant C. Patel** − *Department of Chemistry, Shri Alpesh N. Patel Post Graduate Institute of Science and Research, Anand, Gujarat 388001, India*

**Ankitkumar J. Patel** − *Department of Chemistry, Shri Alpesh N. Patel Post Graduate Institute of Science and Research, Anand, Gujarat 388001, India*

**Nirav H. Bhavsar** − *Department of Microbiology, Shri Alpesh N. Patel Post Graduate Institute of Science and Research, Anand, Gujarat 388001, India*

**Hiteshkumar V. Patel** − *Department of Biochemistry, Shri Alpesh N. Patel Post Graduate Institute of Science and Research, Anand, Gujarat 388001, India*

Complete contact information is available at: https://pubs.acs.org/10.1021/acsomega.4c02007


### Author Contributions

Synthesis and spectral characterization were performed by P.M.T., J.D.P., R.J.P., A.B.D., V.C.P., and A.J.P., thermal analysis was carried out by S.H.C. and A.J.K., and biological activities were conducted by Y.H.V., A.P.C., N.H.B., and H.V.P. J.D.P. and P.M.T. both contributed to the writing, review, and editing of the manuscript.

### Notes

The work does not include any statements that are offensive or illegal, violate anybody else's rights, or contain any information that could lead to harm or injury.

The authors declare no competing financial interest.

## ACKNOWLEDGMENTS

We express our gratitude to the Microbiology Department at Shri Alpesh N. Patel Post Graduate Institute of Science and

Research for their support in the biological aspect of the paper. Additionally, we appreciate the assistance from the P.G. Department of Physics, Sardar Patel University, regarding the thermal properties section. We are also thankful to CIST, Sardar Patel University, for their aid in conducting cytotoxicity activity. Also, we affirm that this work was carried out without receiving any external funding.

## ■ ABBREVIATIONS AND SYMBOLS

| | |
|---|---|
| **SBL** | Schiff base ligand |
| **MTT** | 3-(4,5-dimethylthiazol-2-yl)-2,5-diphenyl tetrazolium bromide |
| **$IC_{50}$** | half-maximal inhibitory concentration |
| **TGA** | thermogravimetric analysis |
| **DTA** | differential thermal analysis |
| **TG** | thermogravimetric |
| **NMR** | nuclear magnetic resonance |
| **IR** | infrared |
| **XRD** | X-ray diffraction |
| **$^1$H NMR** | proton nuclear magnetic resonance |
| **$^{13}$C NMR** | carbon nuclear magnetic resonance |
| ***C. elegans*** | *Caenorhabditis elegans* |
| **LC-MS/MS** | liquid chromatography−mass spectrometry |
| **SEM** | scanning electron microscopy |
| **FTIR** | Fourier-transform infrared spectroscopy |
| **$\mu$M** | micromolar |
| **°C** | degree Celsius |
| **$\mu$L** | microliter |
| **TLC** | thin-layer chromatography |
| **M.P.** | melting point |
| **RCSB** | Research Collaboratory for Structural Bioinformatics |
| **FWO** | Flynn−Wall−Ozawa |
| **FR** | Friedman |
| **NO** | nitrogen oxide radical scavenging |
| **TZD** | thiazolidinediones |
| **$LC_{50}$** | lethal concentration 50 |
| **UV** | ultraviolet |
| **3D** | three-dimensional |
| **AU** | arbitrary unit |
| **Nm** | nanometer |
| ***m*/*z*** | mass-to-charge ratio |
| **Ppm** | parts per million |
| **DMSO-$d_6$** | deuterated dimethyl sulfoxide |
| **$E_a$** | activation energy |
| **CR** | Coats−Redfern |
| **fwhm** | full-width at half-maximum |
| **MDR** | multidrug-resistant |
| **$\Delta S^*$** | change in entropy |
| **mM** | millimolar |
| **PDB** | Protein Data Bank |
| **KAS** | Kissinger−Akahira−Sunose |
| **MMFF** | Merck Molecular Force Field |
| **$\Delta G^*$** | Gibbs free energy change |
| ***A*** | phonon frequency factor |
| **$\Delta H^*$** | activation enthalpy |
| **OPC** | oligomeric proanthocyanidins |

## ■ REFERENCES

(1) Bayeh, Y.; Mohammed, F.; Gebrezgiabher, M.; Elemo, F.; Getachew, M.; Thomas, M. Synthesis, Characterization and Antibacterial Activities of Polydentate Schiff Bases, Based on Salicylaldehyde. *Adv. Biol. Chem.* **2020**, *10* (05), 127−139.

(2) Ommenya, F. K.; Nyawade, E. A.; Andala, D. M.; Kinyua, J. Synthesis, Characterization and Antibacterial Activity of Schiff Base, 4-Chloro-2-{(E)-[(4-Fluorophenyl)Imino]Methyl}phenol Metal (II) Complexes. *J. Chem.* **2020**, *2020*, 1.

(3) Sheikhshoaie, I.; Lotfi, N.; Sieler, J.; Krautscheid, H.; Khaleghi, M. Synthesis, Structures and Antimicrobial Activities of Nickel(II) and Zinc(II) Diaminomaleonitrile-Based Complexes. *Transit. Met. Chem.* **2018**, *43* (6), 555−562.

(4) Ferreira, S. B.; Dantas, T. B.; de Figuerêdo Silva, D.; Ferreira, P. B.; de Melo, T. R.; de Oliveira Lima, E. In Silico and in Vitro Investigation of the Antifungal Activity of Isoeugenol against Penicillium Citrinum. *Curr. Top. Med. Chem.* **2019**, *18* (25), 2186−2196.

(5) Fonkui, T. Y.; Ikhile, M. I.; Njobeh, P. B.; Ndinteh, D. T. Benzimidazole Schiff Base Derivatives: Synthesis, Characterization and Antimicrobial Activity. *BMC Chem.* **2019**, *13* (1), 1−11.

(6) Claudel, M.; Schwarte, J. V.; Fromm, K. M. New Antimicrobial Strategies Based on Metal Complexes. *Chemistry (Easton).* **2020**, *2* (4), 849−899.

(7) Haj, N. Q.; Mohammed, M. O.; Mohammood, L. E. Synthesis and Biological Evaluation of Three New Chitosan Schiff Base Derivatives. *ACS Omega* **2020**, *5* (23), 13948−13954.

(8) Nyawade, E. A.; Onani, M. O.; Meyer, S.; Dube, P. Synthesis, Characterization and Antibacterial Activity Studies of New 2-Pyrral-L-Amino Acid Schiff Base Palladium (II) Complexes. *Chem. Pap.* **2020**, *74* (11), 3705−3715.

(9) Odularu, A. T. Ease to Challenges in Achieving Successful Synthesized Schiff Base, Chirality, and Application as Antibacterial Agent. *Biomed Res. Int.* **2023**, *2023* (3), 1.

(10) Lemilemu, F.; Bitew, M.; Demissie, T. B.; Eswaramoorthy, R.; Endale, M. Synthesis, Antibacterial and Antioxidant Activities of Thiazole-Based Schiff Base Derivatives: A Combined Experimental and Computational Study. *BMC Chem.* **2021**, *15* (1), 1−18.

(11) Afzal, H. R.; Khan, N. U. H.; Sultana, K.; Mobashar, A.; Lareb, A.; Khan, A.; Gull, A.; Afzaal, H.; Khan, M. T.; Rizwan, M.; Imran, M. Schiff Bases of Pioglitazone Provide Better Antidiabetic and Potent Antioxidant Effect in a Streptozotocin-Nicotinamide-Induced Diabetic Rodent Model. *ACS Omega* **2021**, *6* (6), 4470−4479.

(12) Szklarzewicz, J.; Jurowska, A.; Hodorowicz, M.; Kazek, G.; Mordyl, B.; Menaszek, E.; Sapa, J. Characterization and Antidiabetic Activity of Salicylhydrazone Schiff Base Vanadium(IV) and (V) Complexes. *Transit. Met. Chem.* **2021**, *46* (3), 201−217.

(13) Hassan, A. M.; Said, A. O.; Heakal, B. H.; Younis, A.; Aboulthana, W. M.; Mady, M. F. Green Synthesis, Characterization, Antimicrobial and Anticancer Screening of New Metal Complexes Incorporating Schiff Base. *ACS Omega* **2022**, *7* (36), 32418−32431.

(14) Subin Kumar, K. Design, One-Pot Synthesis, Cytotoxic, in Vivo Anticancer, Antioxidant and Antimicrobial Evaluation of a Novel Mixed Schiff Base Ligand and Its Metal Complexes. *Results Chem.* **2022**, *4*, No. 100463.

(15) Manjare, S. B.; Mahadik, R. K.; Manval, K. S.; More, P. P.; Dalvi, S. S. Microwave-Assisted Rapid and Green Synthesis of Schiff Bases Using Cashew Shell Extract as a Natural Acid Catalyst. *ACS Omega* **2023**, *8*, 473.

(16) Odularu, A. T. Manganese Schiff Base Complexes, Crystallographic Studies, Anticancer Activities, and Molecular Docking. *J. Chem.* **2022**, *2022*, 1.

(17) Drake, J.; Link, C. D.; Butterfield, D. A. Oxidative Stress Precedes Fibrillar Deposition of Alzheimer's Disease Amyloid $\beta$-Peptide (1−42) in a Transgenic Caenorhabditis Elegans Model. *Neurobiol. Aging* **2003**, *24* (3), 415−420.

(18) Lai, C. H.; Chou, C. Y.; Ch'ang, L. Y.; Liu, C. S.; Lin, W. C. Identification of Novel Human Genes Evolutionarily Conserved in Caenorhabditis Elegans by Comparative Proteomics. *Genome Res.* **2000**, *10* (5), 703−713.

(19) Boruah, J. J.; Bhatt, Z. S.; Nathani, C. R.; Bambhaniya, V. J.; Guha, A. K.; Das, S. P. Green Synthesis of a Vanadium(V) Schiff Base Complex by Grinding Method: Study on Its Catalytic and Anti-Bacterial Activity. *J. Coord. Chem.* **2021**, *74* (12), 2055−2068.



https://doi.org/10.1021/acsomega.4c02007
*ACS Omega* 2024, 9, 35431−35448

(20) Sravanthi, M.; Kavitha, B.; Reddy, P. S. Green Route for Efficient Synthesis of Biologically Active Schiff Base Ligand Derived From 2 − Hydroxy Acetophenone: Structural, Spectroscopic, Anti Microbial and Molecular Modeling Studies. *Int. Res. J. Pharm.* **2019**, *10* (3), 215−220.
(21) Gundlewad, G. B. Green Synthesis of Schiff Bases by Using Natural Acid Catalysts. *Int. J. Res. Appl. Sci. Eng. Technol.* **2022**, *10* (7), 457−460.
(22) Ayuk, E. L.; Okoro, U. C.; Ugwur, M. O. A Review on Biological Catalysts in Organic Synthesis. *Int. J. Adv. Eng. Res. Appl.* **2016**, *2* (6), 296−321.
(23) Bougossa, I.; Aggoun, D.; Ourari, A.; Berenguer, R.; Bouacida, S.; Morallon, E. Synthesis and Characterization of a Novel Non-Symmetrical Bidentate Schiff Base Ligand and Its Ni(II) Complex: Electrochemical and Antioxidant Studies. *Chem. Pap.* **2020**, *74* (11), 3825−3837.
(24) Kaya, İ.; Daban, S.; Şenol, D. Synthesis and Characterization of Schiff Base, Co(II) and Cu(II) Metal Complexes and Poly(Phenoxy-Imine)s Containing Pyridine Unit. *Inorg. Chim. Acta* **2021**, *515*, No. 120040.
(25) Bashiri, M.; Jarrahpour, A.; Nabavizadeh, S. M.; Karimian, S.; Rastegari, B.; Haddadi, E.; Turos, E. Potent Antiproliferative Active Agents: Novel Bis Schiff Bases and Bis Spiro *β*-Lactams Bearing Isatin Tethered with Butylene and Phenylene as Spacer and DNA/BSA Binding Behavior as Well as Studying Molecular Docking. *Med. Chem. Res.* **2021**, *30* (1), 258−284.
(26) Knittl, E. T.; Abou-Hussein, A. A.; Linert, W. Syntheses, Characterization, and Biological Activity of Novel Mono- and Binuclear Transition Metal Complexes with a Hydrazone Schiff Base Derived from a Coumarin Derivative and Oxalyldihydrazine. *Monatshefte fur Chemie* **2018**, *149* (2), 431−443.
(27) Kadhem, B. J.; Alshawi, J.; Alsalim, T. A.; Abdalla, M. Novel Schiff Bases Ligands and Their Complexes: Thermal Analysis Antibacterial Activity, and Molecular Docking. *Egypt. J. Chem.* **2022**, *65* (7), 107−119.
(28) Omer, A. M.; Eltaweil, A. S.; El-Fakharany, E. M.; Abd El-Monaem, E. M.; Ismail, M. M. F.; Mohy-Eldin, M. S.; Ayoup, M. S. Novel Cytocompatible Chitosan Schiff Base Derivative as a Potent Antibacterial, Antidiabetic, and Anticancer Agent. *Arab. J. Sci. Eng.* **2023**, *48* (6), 7587−7601.
(29) Ali, S.; Zheng, H.; Zaidi, A.; Ahmed Khan, F.; Majid Bukhari, S.; Riaz, M.; Mumtaz Khan, M.; Sammi, S.; U-Llah, I.; Amin, A.; Jahangir, M. Moxifloxacin Metal Complexes: Synthesis, Characterisation, Antimicrobial and Antidiabetic Activities with Docking Studies. *Bioinorg. Chem. Appl.* **2023**, *2023*, 1.
(30) Hunt, P. R.; The, C. Elegans Model in Toxicity Testing. *J. Appl. Toxicol.* **2017**, *37* (1), 50−59.
(31) Thakor, P. M.; Patel, R. J.; Giri, R. K.; Chaki, S. H.; Khimani, A. J.; Vaidya, Y. H.; Thakor, P.; Thakkar, A. B.; Patel, J. D. Synthesis, Spectral Characterization, Thermal Investigation, Computational Studies, Molecular Docking, and In Vitro Biological Activities of a New Schiff Base Derived from 2 - Chloro Benzaldehyde and 3,3'-Dimethyl-[1,1'-biphenyl]-4,4'-diamine. *ACS Omega* **2023**, 33069.
(32) Thakor, P.M.; Patel, R. J.; Vaidya, Y. H.; Verma, D. N.; Patel, J. D. Natural acid-catalyzed synthesis of 6,6'-(((3,3'-dimethoxy-[1,1'-biphenyl]-4,4'-Diyl) bis (azanylylidene)) bis (methanylylidene)) bis (2, 4-dichlorophenol), its conventionally synthesized metal complexes and their potential as biological agents. *Rasayan J. Chem.* **2023**, *16* (1), 61−68, DOI: 10.31788/RJC.2023.1618108.
(33) Lankisch, M.; Layer, P.; Rizza, R. A.; DiMagno, E. P. Acute Postprandial Gastrointestinal and Metabolic Effects of Wheat Amylase Inhibitor (WAI) in Normal, Obese, and Diabetic Humans. *Pancreas* **1998**, *17* (2), 176−181.
(34) Roux, M. J.; Martínez-Maza, R.; Le Goff, A.; López-Corcuera, B.; Aragón, C.; Supplisson, S. The Glial and the Neuronal Glycine Transporters Differ in Their Reactivity to Sulfhydryl Reagents. *J. Biol. Chem.* **2001**, *276* (21), 17699−17705.
(35) Bernfeld, P. Amylass, *α* and *β*. *Methods Enzym.* **1955**, *1*, 149−158.
(36) Taha, M.; Irshad, M.; Imran, S.; Rahim, F.; Selvaraj, M.; Almandil, N. B.; Mosaddik, A.; Chigurupati, S.; Nawaz, F.; Ismail, N. H.; Ibrahim, M. Thiazole Based Carbohydrazide Derivatives as *α*-Amylase Inhibitor and Their Molecular Docking Study. *Heteroat. Chem.* **2019**, *2019*, No. 7502347.
(37) Yousuf, S.; Khan, K. M.; Salar, U.; Chigurupati, S.; Muhammad, M. T.; Wadood, A.; Aldubayan, M.; Vijayan, V.; Riaz, M.; Perveen, S. 2′-Aryl and 4′-Arylidene Substituted Pyrazolones: As Potential *α*-Amylase Inhibitors. *Eur. J. Med. Chem.* **2018**, *159*, 47−58.
(38) Ramírez-Escudero, M.; Gimeno-Pérez, M.; González, B.; Linde, D.; Merdzo, Z.; Fernández-Lobato, M.; Sanz-Aparicio, J. Structural Analysis of *β*-Fructofuranosidase from Xanthophyllomyces Dendrorhous Reveals Unique Features and the Crucial Role of N-Glycosylation in Oligomerization and Activity. *J. Biol. Chem.* **2016**, *291* (13), 6843−6857.
(39) Allouche, A.-R. Software News and Updates Gabedit — A Graphical User Interface for Computational Chemistry Softwares. *J. Comput. Chem.* **2011**, *32*, 174−182.
(40) Singhal, S.; Khanna, P.; Khanna, L. Synthesis, DFT Studies, Molecular Docking, Antimicrobial Screening and UV Fluorescence Studies on Ct-DNA for Novel Schiff Bases of 2-(1-Aminobenzyl) Benzimidazole. *Heliyon* **2019**, *5* (10), No. e02596.
(41) Namera, D. L.; Thakkar, S. S.; Thakor, P.; Bhoya, U.; Shah, A. Arylidene Analogues as Selective COX-2 Inhibitors: Synthesis, Characterization, in Silico and in Vitro Studies. *J. Biomol. Struct. Dyn.* **2021**, *39* (18), 7150−7159.
(42) Halgren, T. A. MMFF VI. MMFF94s Option for Energy Minimization Studies. *J. Comput. Chem.* **1999**, *20* (7), 720−729.
(43) Thakor, P.; Subramanian, R. B.; Thakkar, S. S.; Ray, A.; Thakkar, V. R. Phytol Induces ROS Mediated Apoptosis by Induction of Caspase 9 and 3 through Activation of TRAIL, FAS and TNF Receptors and Inhibits Tumor Progression Factor Glucose 6 Phosphate Dehydrogenase in Lung Carcinoma Cell Line (A549). *Biomed. Pharmacother.* **2017**, *92*, 491−500.
(44) Gajera, H. P.; Hirpara, D. G.; Katakpara, Z. A.; Patel, S. V.; Golakiya, B. A. Molecular Evolution and Phylogenetic Analysis of Biocontrol Genes Acquired from SCoT Polymorphism of Mycoparasitic Trichoderma Koningii Inhibiting Phytopathogen Rhizoctonia Solani Kuhn. *Infect. Genet. Evol.* **2016**, *45*, 383−392.
(45) Amaral, L. de O.; Lima, V. S.; Soares, S. M.; Bornhorst, J.; Lemos, S. S.; Gatto, C. C.; Burrow, R. A.; Gubert, P. Synthesis, Structural Characterization and Evaluation of the Chelating Potential in C. Elegans Involving Complexes of Mercury (II) with Schiff Bases Derived from Amino Acids. *J. Organomet. Chem.* **2020**, *926*, No. 121500.
(46) Apfeld, J.; Alper, S. What Can We Learn about Human Disease from the Nematode C. Elegans? *Methods Mol. Biol.* **2018**, *1706*, 53−75.
(47) Faraki, Z.; Bodaghifard, M. A. Synthesis and Characterization of a Highly Functionalized Cationic Porous Organic Polymer as an Efficient Adsorbent for Removal of Hazardous Nitrate and Chromate Ions. *Results Chem.* **2022**, *4*, No. 100657.
(48) Suneetha, G.; Ayodhya, D.; Sunitha Manjari, P. Schiff Base Stabilized Gold Nanoparticles: Synthesis, Characterization, Catalytic Reduction of Nitroaromatic Compounds, Fluorometric Sensing, and Biological Activities. *Results Chem.* **2023**, *5*, No. 100688.
(49) Bartyzel, A. Synthesis, Thermal Behaviour and Some Properties of CuII Complexes with N,O-Donor Schiff Bases. *J. Therm. Anal. Calorim.* **2018**, *131* (2), 1221−1236.
(50) Patterson, A. L. The Scherrer Formula for X-Ray Particle Size Determination. *Phys. Rev.* **1939**, *56* (10), 978−982.
(51) Giri, R. K.; Chaki, S.; Khimani, A. J.; Vaidya, Y. H.; Thakor, P.; Thakkar, A. B.; Pandya, S. J.; Deshpande, M. P. Biocompatible CuInS2Nanoparticles as Potential Antimicrobial, Antioxidant, and Cytotoxic Agents. *ACS Omega* **2021**, *6* (40), 26533−26544.
(52) Malek, T. J.; Chaki, S. H.; Giri, R. K.; Deshpande, M. P. The Structural, Morphological, and Optical Study of Chemical Bath Deposition and a Spin Coating Deposited Mackinawite FeS Thin Films. *Appl. Phys. A: Mater. Sci. Process.* **2022**, *128* (9), 830.


https://doi.org/10.1021/acsomega.4c02007
*ACS Omega* 2024, 9, 35431−35448

(53) Kannaujiya, R. M.; Chaki, S. H.; Khimani, A. J.; Parekh, Z. R.; Deshpande, M. P. Kinetic Stability of Tin Telluride Nanoparticles Synthesized by Hydrothermal Method. *Chem. Thermodyn. Therm. Anal.* **2022**, *6* (April), No. 100058.
(54) Giri, R. K.; Chaki, S. H.; Khimani, A. J.; Deshpande, M. P. Mechanistic Insights into Transport Properties of Chemical Vapour Transport Grown CuInS2 Single Crystal. *J. Alloys Compd.* **2023**, *959*, No. 170487.
(55) Giri, R. K.; Chaki, S. H.; Khimani, A. J.; Patel, S. R.; Deshpande, M. P. Thermal Investigation of Nanospheres and Nanowhiskers of CuInS2. *Eur. Phys. J. Plus* **2021**, *136* (3), 320.
(56) Fernandez, A.; Ortiz, L. R.; Asensio, D.; Rodriguez, R.; Mazza, G. Kinetic Analysis and Thermodynamics Properties of Air/Steam Gasification of Agricultural Waste. *J. Environ. Chem. Eng.* **2020**, *8*, No. 103829.
(57) Kissinger, H. E. Reaction Kinetics in Differential Thermal Analysis. *Anal. Chem.* **1957**, *29* (11), 1702−1706.
(58) Akahira, T. Trans. Joint Convention of Four Electrical Institutes. *Res. Rep. Chiba Inst. Technol.* **1971**, *16*, 22−31.
(59) COATS, A. W.; REDFERN, J. P. Kinetic Parameters from Thermogravimetric Data. *Nature* **1964**, *201* (4914), 68−69.
(60) Fernandez, A.; Sette, P.; Echegaray, M.; Soria, J.; Salvatori, D.; Mazza, G.; Rodriguez, R. Clean Recovery of Phenolic Compounds, Pyro-Gasification Thermokinetics, and Bioenergy Potential of Spent Agro-Industrial Bio-Wastes. *Biomass Convers. Biorefin.* **2022**, *13*, 12509−12526.
(61) Ozawa, T. Estimation of Activation Energy by Isoconversion Methods. *Thermochim. Acta* **1992**, *203*, 159−165.
(62) Abu-Sehly, A. A. Variation of the Activation Energy of Crystallization in Se81.5Te16Sb2.5 Chalcogenide Glass: Isoconversional Analysis. *Thermochim. Acta* **2009**, *485* (1−2), 14−19.
(63) Friedman, H. L. Kinetics of Thermal Degradation of Char-Forming Plastics from Thermogravimetry. Application to a Phenolic Plastic. *J. Polym. Sci. Part C Polym. Symp.* **1964**, *6* (1), 183−195.
(64) Khimani, A. J.; Chaki, S. H.; Giri, R. K.; Meena, R. R.; Kannaujiya, R. M.; Deshpande, M. P. Thermal Exploration of Sonochemically Achieved SnS2 Nanoparticles: Elemental, Structural, and Morphological Investigations of TG Residual SnS2. *Chem. Thermodyn. Therm. Anal.* **2023**, *9*, No. 100104.
(65) Park, H. E. H.; Jung, Y.; Lee, S. J. V. Survival Assays Using Caenorhabditis Elegans. *Mol. Cells* **2017**, *40* (2), 90−99.


https://doi.org/10.1021/acsomega.4c02007
*ACS Omega* 2024, 9, 35431−35448